TimeSeAD: Benchmarking Deep Time-Series Anomaly Detection

Anonymous authors
Paper under double-blind review

Abstract

Developing new methods for detecting anomalies in time series is of great practical significance, but progress is hindered by the difficulty of assessing the benefit of new methods, for the following reasons. (1) Public benchmarks are flawed (e.g., due to questionable anomaly labels), (2) there is no widely accepted standard evaluation metric, and (3) evaluation protocols are mostly inconsistent. In this work, we address all three issues: (1) We critically analyze several of the most widely-used multivariate datasets, identify a number of significant issues, and select the best candidates for evaluation. (2) We introduce a new evaluation metric for time-series anomaly detection, which—in contrast to previous metrics—is recall consistent and takes temporal correlations into account. (3) We analyze and overhaul existing evaluation protocols and provide the largest benchmark of deep multivariate time-series anomaly detection methods to date. We focus on deep-learning based methods and multivariate data, a common setting in modern anomaly detection. We provide all implementations and analysis tools in a new comprehensive library for `Time Se`ries `A`nomaly `D`etection, called `TimeSeAD`[1].

1 Introduction

Anomaly detection (AD) on time series is a fundamental problem in machine learning and significant in various applications, from monitoring patients and uncovering financial fraud to detecting faults in manufacturing and critical process conditions in chemical plants (Ruff et al., 2021). The aim in AD is to automatically identify significant deviations to the norm—so-called *anomalies*. There are two principal approaches to AD on time series: An anomaly detector assigns a score either to each time step separately (point-wise) or the entire time series (globally). This work focuses on the point-wise setting, but the methods developed for it can also be applied to the global setting by aggregating the local labels.

Evaluating the accuracy of an anomaly detector for time series is not straightforward. Most authors apply point-wise metrics, particularly the $F1$-score, which has become a standard in recent years. However, time series exhibit complex temporal dependencies not found in other data. Point-wise metrics ignore these dependencies, which may lead to incorrect results. The few prior attempts to introduce specialized evaluation metrics for time-series AD have not caught on in the community, primarily due to their complexity and the counterintuitive results they can produce.

Beyond inadequate metrics, the other major problem in time-series AD is the data. Recently, Wu & Keogh (2021) have exposed major flaws in many widely used univariate datasets, ranging from surface-level issues (such as mislabeled points) to deep-rooted problems (such as positional bias and trivial features). These flaws alone invalidate many evaluations and present an impossible-to-ignore hurdle for the field. The present work shows that such (and other) flaws are also prevalent in multivariate datasets, particularly in high-dimensional ones. As a result, there exists no sound, comprehensive analysis of AD on multivariate times-series data yet.

[1]We provide the code in the supplementary material, and later through a GitHub link.

The distinct flaws of datasets, metrics, and evaluation protocols complicate any comparison and make it hard to determine any meaningful progress in the field. This work examines the most popular datasets, metrics, and evaluation protocols in detail and proposes a general evaluation framework to address the identified problems. We have created a detailed, extendable, and user-friendly library, where we implemented 25 deep-learning based multivariate time-series AD methods. This library is an unprecedented asset enabling researchers to quickly and reliably develop, test, and evaluate new methods. It provides a set of tools to analyze datasets and methods alike.

Our main contributions are the following:

- We conduct a **thorough analysis** of the most widely used **datasets, metrics, and evaluation protocols** for multivariate time-series AD, revealing significant problems with all three.
- We propose a **new evaluation metric** that is provably recall consistent and empirically provides a reasonable ordering of evaluated methods.
- We present the **largest comprehensive benchmark so far** for multivariate time-series AD, comparing 25 deep-learning methods on 21 datasets.

2 Related Work

Several papers have attempted to summarize the vast number of time-series AD approaches. However, most prior work is focused either on a subclass of network architectures (Lindemann et al., 2021; Lee et al., 2021; Wen et al., 2022) or on a specific application domain and methods specifically applied therein (Luo et al., 2021). Others discuss multiple methods and concepts in a high-level overview (Blázquez-García et al., 2021), with a strong focus on application. Choi et al. (2021) use point-wise metrics to selectively evaluate some methods on three datasets that we find being problematic (see Section 3.1). Other papers have evaluated small selections of methods in a similar setting (Lai et al., 2021; Audibert et al., 2022).

Schmidl et al. (2022) evaluate a large collection of more than 20 deep and several shallow methods primarily on univariate or low-dimensional datasets. However, deep methods truly shine in high-dimensional settings (analyzed in the present paper). Their evaluation relies on a slow (quadratic in time) implementation of time-series precision and recall (Tatbul et al., 2018). Speed is essential in deep learning, which is known to be computation-heavy. As a result, they excluded results where the computation took too long. Other libraries mostly focus on shallow or basic deep methods (Bhatnagar et al., 2021).

For the analysis of datasets, we build upon the work of Wu & Keogh (2021). They thoroughly analyzed several of the most popular univariate time-series datasets, identified multiple flaws, and concluded that many datasets do not allow for fair evaluation of AD algorithms. Following their work, we find several similar problems with the most widely used multivariate time-series datasets.

Overcoming the inherent problems of point-wise metrics on time-series data is no easy task. Huet et al. (2022) provide an overview of existing attempts and introduce a metric based on the distance of predicted anomaly windows to the nearest anomaly. They report their results on datasets, in which we identify several problems. Others modify the predictions before evaluation (Xu et al., 2018; Scharwächter & Müller, 2020; Kim et al., 2022) or consider only the beginning of anomaly windows (Doshi et al., 2022). Some metrics are clearly biased towards extreme cases of anomaly detectors (Hundman et al., 2018). Lavin & Ahmad (2015) introduced the first metric to directly address the problems of point-wise evaluations by penalizing late predictions in anomaly windows. With its numerous hyperparameters, the metric was too complex and varied to be widely adapted (Xu et al., 2018). Tatbul et al. (2018) proposed time-series precision and recall, a generalization of previous concepts in many ways. For a long time, the only publicly available implementations were too slow and cumbersome to use in practice. Garg et al. (2021) propose a variation of time-series precision and recall that ignores any overlap between prediction and anomalies in the recall.

3 The Illusion of Progress

In this section, we uncover several issues that are causing evaluations in (multivariate) time-series AD to be unreliable, resulting in an illusion of progress. Our analysis first examines some of the most commonly used datasets, SWaT (Goh et al., 2016), WADI (Ahmed et al., 2017), and SMAP and MSL (Hundman et al., 2018). These datasets are the backbone of time-series AD evaluation and have been used in virtually all major comparisons in the field (Schmidl et al., 2022; Garg et al., 2021; Choi et al., 2021; Jacob et al., 2020). Our analysis reveals several significant flaws in these datasets. Second, we investigate the shortcomings of frequently used evaluation metrics, particularly the $F1$-score and its adaptations. Lastly, we examine the inconsistencies and other problems within established evaluation protocols.

3.1 Datasets

In the following, we outline several general problems found in time-series datasets and summarize our findings on SWaT, WADI, SMAP, and MSL[2].

Anomaly density refers to the fraction of anomalies in the test set. Anomalies are usually rare deviations and their density in the test set should reflect this. However, with the exception of WADI, all datasets contain $\geq 10\%$ anomalies, which is too high to be representative of realistic scenarios. Ideally, the anomaly density should be $\leq 5\%$.

Positional bias is introduced when the distribution of the relative positions of anomalies deviates significantly from a uniform distribution. For example, anomalies can be biased towards the end, when an anomaly means a fatal error for the generating process (Wu & Keogh, 2021). Any algorithm accounting for this shift has an immediate advantage over its competitors. To investigate this bias, we examine the relative positions of anomalous time steps in each time series in the test sets and find clear positional bias in both SMAP and MSL (see Figure 1a).

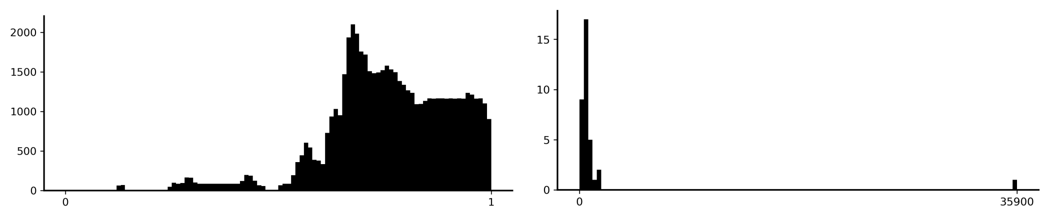

(a) Histogram of relative anomaly positions (b) Histogram of anomaly window lengths

Figure 1: (a) The relative positions of anomalies in the test set of SMAP show clear positional bias towards the latter half of the time series. (b) The distribution of anomaly window lengths in SWaT shows the existence of exceptionally long anomaly windows.

Long anomalies can introduce problems in the evaluation. Some methods may rely on normal context in each window to predict subsequent anomalies and are thus at a disadvantage when long anomalies occur. Long anomalies also interact with adapted evaluation protocols, which we discuss in Section 3.3. Although not inherently negative, both effects should be kept in mind when using data containing long anomalies for evaluation. We found that the vast majority of anomalous time steps in all datasets belong to one or several long anomalies (for example, see Figure 1b).

Constant features appear in all datasets. Some datasets have features that remain constant, even throughout both training and test sets (see Figure 2). While such features may be valuable in practical applications, they add unnecessary complexity to the benchmark.

Distributional shift between normal training and test data breaks one of the fundamental assumptions of AD. For an unbiased and fair evaluation, anomalies should be labeled, where they occur in the data. Effects that show in a sensor only after the labeled anomaly (see

[2]We provide descriptions and detailed examples for all datasets in Appendix B.

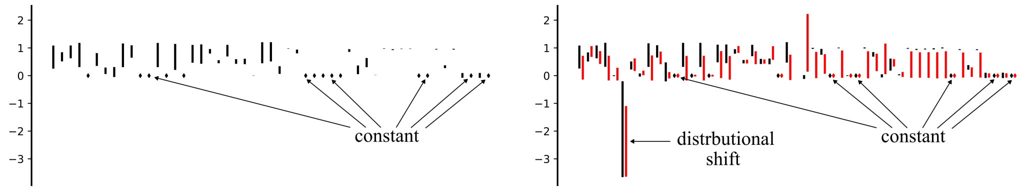

(a) Train set feature distribution

(b) Test set feature distribution

Figure 2: Mean and standard deviation of features in SWaT for normal points (black) and anomalies (red), reveal several features that are constant across the entire dataset and one particular feature for which the normal points experience clear distributional shift between training and test set.

Figure 3a) pose an impossible problem for any anomaly detector. This holds especially true for long-lasting changes in the data, often permanently changing the distribution of the system (see Figure 3b)[3].

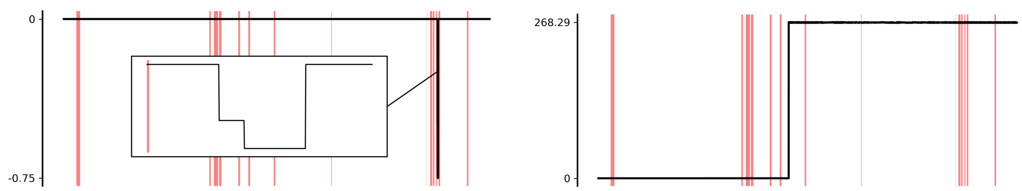

(a) 2_P_004_SPEED

(b) 2A_AIT_002_PV

Figure 3: Two features from the test set of WADI show where anomalies seem to cause (a) delayed or (b) long-term effects in the data. Red shaded areas are ground truth anomalies. The feature in (b), normalized to range in $[0, 1]$ on the training set, jumps to unprecedented values on the test set.

SWaT and WADI contain the clearest examples of delayed and long-term effects in the data, where the distribution changes drastically in the second half of the test set. We found exceptionally long anomalies in both datasets, especially in SWaT. Thus evaluations on these two datasets are highly unreliable. In our opinion, they are not suited for AD evaluation.

SMAP and MSL contain time series with one feature representing a sensor measurement, while the rest represent binary encoded commands. The command features are often constant, in particular in sections where anomalies occur. Furthermore, since several sensors have been used to construct the dataset, each time series in both datasets should be considered separately. SMAP contains a clear positional bias towards the end, and both seem to include significant distributional shifts caused by anomalies. Thus both MSL and SMAP are not suited for general AD evaluation in their current iteration.

3.2 Metrics

An anomaly detector produces an anomaly score for each time point in a time series. Anomalies are then predicted by thresholding these scores. Point-wise metrics consider each prediction separately, with the point-wise $F1$-score as the most popular choice, oftentimes reported alongside precision and recall. Ignoring the temporal dependency between time steps comes at a price: Any two methods that differ only in a predictive pattern (the structure of their predictions) on some anomaly window are indistinguishable for any point-wise metric (see Figure 4a as an example). Predictive patters matter for separating early and late or consistent and fragmented predictions, and their differences should be reflected in the metric used to compare them.

Time-series precision and recall (Tatbul et al., 2018) is an attempt to overcome these issues. Consider the set of anomaly windows in a dataset $\mathcal{A}$ and the set of predicted windows $\mathcal{P}$,

[3] For a detailed description, discussion, and more examples, refer to Appendix B.

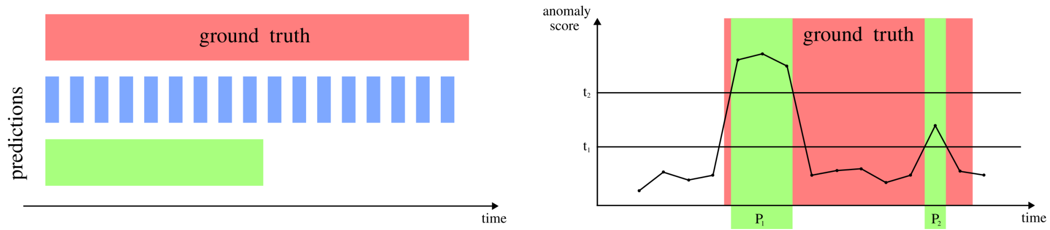

(a) Two predictions of equal size with distinct predictive patterns on an anomaly.

(b) Anomaly score and predictions P_1, P_2, where only the larger persists for both thresholds t_1, t_2.

Figure 4: (a) A point-wise metric cannot distinguish between two methods that differ only in their predictive pattern on anomalies. (b) Counterintuitively, $TRec$ with a constant bias and $\gamma(x) = x^{-1}$ increases when the threshold increases from t_1 to t_2.

and let $\mathcal{P}_A = \{P \in \mathcal{P} \mid |A \cap P| > 0\}$. Then time-series recall is defined as

$$TRec(\mathcal{A}, \mathcal{P}) = \frac{1}{|\mathcal{A}|} \sum_{A \in \mathcal{A}} \left[\alpha \mathbb{1}(|\mathcal{P}_A| > 0) + (1-\alpha)\gamma(|\mathcal{P}_A|) \sum_{P \in \mathcal{P}} \frac{\sum_{t \in P \cap A} \delta(t - \min A, |A|)}{\sum_{t \in A} \delta(t - \min A, |A|)} \right] \quad (1)$$

with weight $0 \leq \alpha \leq 1$, monotone decreasing cardinality function γ with $\gamma(1) = 1$, and bias function $\delta \geq 1$. This metric can generally produce unintuitive results. For example, consider two disjoint predictions $P_1, P_2 \subset A \in \mathcal{A}$ for a threshold λ, such that $\sum_{t \in P_1 \cap A} \delta(t - \min A, |A|) > \sum_{t \in P_2 \cap A} \delta(t - \min A, |A|)$. Then, if there exists a threshold greater than λ such that P_1 is kept intact while P_2 vanishes, $TRec$ increases (see Figure 4b for illustration).

While the point-wise recall is monotonically decreasing with an increasing threshold—a property we entitle *recall consistency*—the example shows that $TRec$ generally is not recall consistent, particularly for the recommended default parameter choices (Tatbul et al., 2018). This behavior is counterintuitive and can lead to problems when computing aggregated metrics that assume recall consistency. To compute the corresponding precision, the positions of $\mathcal{A}$ and $\mathcal{P}$ are exchanged in the computation of the recall, i.e. $TPrec(\mathcal{A}, \mathcal{P}) = TRec(\mathcal{P}, \mathcal{A})$. This choice encourages any algorithm to predict many small anomaly windows, as all predictions are weighted equally, which clearly conflicts with the choice of a decreasing cardinality function. Even though clearly flawed, time-series recall and precision are the best attempts to include the temporal structure of time series in an evaluation metric so far.

3.3 Evaluation Protocol

Alongside various metrics, the actual evaluation protocols are often vastly inconsistent. Beyond preprocessing, feature selection, and data cleaning, Xu et al. (2018) proposed point adjustment to complement the point-wise nature of the $F1$-score. Point adjustment considers any anomaly window with at least one correctly predicted time step predicted correctly. However, even random methods have a decent chance to predict at least one point in larger anomaly windows, where they can easily reach the performance of most complex methods or even outperform them (Kim et al., 2022; Doshi et al., 2022). Despite these flaws, this technique was adopted by many papers (Su et al., 2019; Audibert et al., 2020; Zhao et al., 2020; Zhang et al., 2021; Xiao et al., 2021; Chen et al., 2021; Wang et al., 2021; Challu et al., 2022; Hua et al., 2022; Chambaret et al., 2022; Zhang et al., 2022b;a). Often the use of point-adjustment and preprocessing methods is not definitively disclosed. In combination with a general lack of details and official implementations, this means results are often hard or even impossible to reproduce consistently[4]. Combined with the general inconsistencies across publications, this leads to inconsistent and questionable reports at the very least. We encountered a lot more problems in evaluation protocols when trying to reproduce the results of many papers. Potential problems include hyperpparameters tuned on the test set,

[4]See Appendix C for details on all considered methods.

results aggregated over multiple datasets, and many more such details. It is clear to see, that these inconsistencies further complicate any comparison.

4 TimeSeAD: Benchmarking Deep Multivariate Time-Series AD

In this section, we propose how to benchmark time-series AD methods in a way that mitigates the issues discussed in Section 3. We discuss the strengths and weaknesses of two datasets, SMD (Su et al., 2019) and Exathlon (Jacob et al., 2020) and propose how their flaws can be mitigated. Further, we introduce a modified version of time-series recall that is recall consistent and a modified version of its corresponding precision that addresses its bias. Finally, we discuss our evaluation protocol and implementation.

4.1 Datasets

In the previous section, we uncovered flaws in several commonly used benchmark datasets. However, there are also datasets that are more suited for benchmarking, namely SMD Su et al. (2019) and Exathlon Jacob et al. (2020).

SMD contains 28 time series generated from different processes and thus comprises 28 datasets. Some of its datasets suffer from distributional shift and have been removed from evaluations in the past (Li et al., 2021b). To the best of our knowledge, there is no automatic statistical test to identify distributional shift in time series, thus we rely on manual inspection of all datasets. We exclude several datasets from the final evaluation, where we suspect delayed or long-term effects caused by anomalies, and only report those results in Appendix E. In total, we remove 13 datasets.

Exathlon comprises eight datasets collected from applications run on a cluster. The time series in Exathlon suffer from missing values, which the creators suggest be replaced with default values. This inadvertently injects unlabeled anomalies in the data, where the default values follow a different distribution. Instead, we replace any missing values with the respective preceding value. We omit two applications, one, for which we identify a severe distributional shift, and one with a too small test set, leaving six datasets. Overall, we find several more instances of possible delayed effects and distributional shift, which might be attributed to background effects. Nonetheless, we strongly encourage further careful inspection by application experts.

4.2 Metrics

In Section 3.2 we discussed the potential and shortcomings of $TRec$ and $TPrec$. We propose new default parameters for $TRec$ and a variation of $TPrec$ to address their flaws. Let us first note the discrepancy between the two terms in Equation (1). The first term counts the number of anomaly windows for which at least one point was predicted correctly. In contrast, the second term is entirely concerned with the predictive structure within each anomaly window. Since the first term is completely oblivious to the size of the anomalies, the range of both terms could vary wildly for each task, and the terms would need to be balanced for each task individually. Furthermore, the second term already implicitly acknowledges the existence of anomalies in their overlap. Thus, we suggest to use $\alpha = 0$.

To prevent unintuitive results, we further require any cardinality function to guarantee recall consistency. Thus, we define a class of functions for which recall consistency always holds.

Theorem 1 $TRec$ is recall consistent for any cardinality function of the form

$$\gamma(1, A) = 1, \qquad \gamma(n, A) = \max_{0<m<n} \frac{\sum_{t \in A} \delta(t - \min A, |A|) - n + m}{\sum_{t \in A} \delta(t - \min A, |A|)} \gamma(m, A).$$

Proof: We provide the detailed proof in Appendix A.

Theorem 2 With constant bias the cardinality function has the closed-form solution

$$\gamma^*(n, A) = \left(\frac{|A| - 1}{|A|}\right)^{n-1}.$$

Proof:[5] We show the proposition by induction. First, note that $\gamma^*(n, A) = \left(\frac{|A|-1}{|A|}\right)^0 = 1$. Now assume $\gamma^*(m, A) = \left(\frac{|A|-1}{|A|}\right)^{m-1}$ for all $m \leq n$. Then it holds

$$\begin{aligned}
\gamma^*(n+1, A) &= \max_{0<m<n+1} \frac{\sum_{t\in A} \delta(t - \min A, |A|) - n - 1 + m}{\sum_{t\in A} \delta(t - \min A, |A|)} \gamma(m, A) \\
&= \max_{0<m<n+1} \frac{|A| - n - 1 + m}{|A|} \left(\frac{|A| - 1}{|A|}\right)^{m-1} \\
&\geq \frac{|A| - 1}{|A|} \left(\frac{|A| - 1}{|A|}\right)^{n-1} \\
&= \left(\frac{|A| - 1}{|A|}\right)^{n}
\end{aligned}$$

Furthermore, it holds

$$\begin{aligned}
\gamma^*(n+1, A) &= \max_{0<m<n+1} \frac{\sum_{t\in A} \delta(t - \min A, |A|) - n - 1 + m}{\sum_{t\in A} \delta(t - \min A, |A|)} \gamma(m, A) \\
&\overset{\text{Lemma 1}}{\leq} \max_{0<m<n+1} \left(\frac{|A| - 1}{|A|}\right)^{n+1-m} \left(\frac{|A| - 1}{|A|}\right)^{m-1} \\
&= \left(\frac{|A| - 1}{|A|}\right)^{n}
\end{aligned}$$

□

We call $TRec$ with cardinality function γ^* and constant bias $TRec^*$. The general formulation preserves the bias function as tunable parameter. It is important to retain this degree of generality, as we can still adapt the metric to specific use-cases, such as early prediction.

Finally, we address the bias of time-series precision by weighing each term according to the size of the anomaly. Thus, instead of using equal weights $|\mathcal{P}|^{-1}$, we weigh each term inside the sum by $|P| \left(\sum_{P\in\mathcal{P}} |P|\right)^{-1}$. Using these implementations of precision and recall, we can compute an $F1$-score and the area under precision recall curve (AUPRC). Empirically we find that this $F1$-score produces reasonable orderings of methods, see Figure 5.

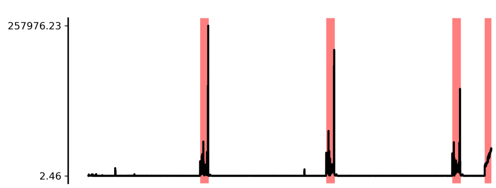

(a) LSTM-P scores

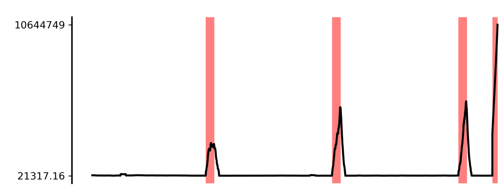

(b) TCN-AE scores

Figure 5: Scores from two different methods on a test time series of Exathlon 2, where (b) performs better according to our score, but worse according to the point-wise $F1$-score, providing an ordering aligned with our intuition.

[5]We provide details on the technical Lemma 1 in Appendix A.

Table 1: Cross-validation results on Exathlon and SMD. We report the ranks according to the best F_1-score based on $TRec^*$ and $TPrec^*$ averaged over all test folds. μ_s^{Exa} and μ_s^{SMD} are the ranked average scores over all datasets in Exathlon and SMD respectively and μ_s^{all} shows the ordering of the weighted average over all datasets from both Exathlon and SMD, weighted by the number of datasets in Exathlon and SMD. We provide the full results in Appendix E.

		Exathlon							**SMD**																
	ID	1	2	4	5	6	9	μ_s^{Exa}	1	6	8	9	10	11	13	14	16	17	20	21	24	26	27	μ_s^{SMD}	μ_s^{all}
reconstruction	LSTM-AE	24	**2**	20	21	21	23	22	4	**3**	5	10	**1**	8	4	**1**	**1**	**3**	**3**	**1**	**2**	4	**3**	**1**	4
	LSTM-Max-AE	5	23	22	19	20	7	20	**3**	22	21	12	21	17	6	18	20	11	21	22	12	7	11	17	22
	MSCRED	10	**1**	**2**	14	**3**	**1**	**1**	8	19	**1**	20	19	24	21	24	13	9	24	21	20	21	18	20	12
	FC-AE	4	20	10	15	13	10	10	7	13	8	9	11	13	9	8	6	6	14	6	9	8	**2**	7	7
	USAD	7	18	9	11	16	19	15	23	20	19	18	20	11	10	10	23	13	12	14	19	22	15	15	16
	TCN-AE	8	5	14	9	18	**2**	**3**	20	15	6	23	22	23	23	22	16	16	5	19	21	**1**	22	21	17
	GenAD	**3**	25	**3**	10	**1**	25	4	19	25	22	24	24	25	8	19	22	18	25	25	18	14	13	24	23
	STGAT-MAD	14	17	8	20	**2**	15	14	12	7	14	4	4	10	14	4	**3**	7	4	10	8	**2**	5	5	**3**
prediction	LSTM-P	19	12	21	8	25	12	24	**1**	**1**	**2**	14	6	9	**2**	**2**	4	**2**	11	7	11	12	4	**2**	10
	LSTM-S2S-P	13	19	**1**	23	12	5	11	6	16	**3**	19	23	21	24	23	10	15	17	17	15	13	20	18	18
	DeepAnt	12	10	6	12	11	13	7	9	12	12	5	17	15	15	9	7	14	10	13	6	10	19	12	11
	TCN-S2S-P	15	7	12	13	23	16	19	15	**2**	4	6	9	7	16	12	**2**	**1**	**2**	5	5	11	**1**	**3**	5
	GDN	**2**	6	16	16	8	4	**2**	**2**	14	7	11	7	14	13	14	15	10	14	11	4	19	10	10	**2**
VAEs	LSTM-VAE	20	14	13	**2**	7	17	6	14	11	17	21	**2**	5	7	13	9	20	8	**2**	7	23	14	9	8
	Donut	23	22	7	4	19	9	16	16	6	9	**3**	**3**	6	19	5	18	5	**1**	9	**1**	24	9	6	6
	LSTM-DVAE	18	24	17	3	22	18	17	24	10	15	22	8	4	18	**3**	12	23	9	**3**	10	20	23	13	13
	GMM-GRU-VAE	21	11	18	6	5	**3**	5	10	5	11	**2**	5	**1**	17	6	14	4	6	8	**3**	15	6	4	**1**
	OmniAnomaly	25	21	25	**1**	4	11	21	17	4	16	8	16	**2**	**1**	15	5	21	18	15	14	25	7	11	14
	SIS-VAE	17	16	5	7	6	21	12	5	9	10	7	12	12	11	7	8	8	7	12	13	**3**	8	8	9
GANs	BeatGAN	6	**3**	15	18	14	14	8	18	18	18	15	13	16	12	17	21	12	16	16	22	17	17	16	15
	MAD-GAN	9	15	11	22	9	22	18	21	21	13	17	18	22	22	16	17	24	13	23	25	18	25	23	24
	LSTM-VAE-GAN	11	8	4	24	15	6	13	13	17	20	**1**	15	19	**3**	21	24	22	21	18	24	6	12	19	20
	TADGAN	**1**	4	19	17	17	20	9	11	24	25	16	14	20	5	20	19	17	19	20	17	5	24	22	21
other	LSTM-AE OC-SVM	16	9	23	25	24	24	25	25	23	23	25	25	18	25	25	25	19	23	24	23	9	16	25	25
	MATD-GAT	22	13	24	5	10	8	23	22	8	24	13	10	**3**	20	11	11	25	20	4	16	16	21	14	19

4.3 Evaluation

To ensure a fair evaluation, we implemented, trained, and evaluated all methods and datasets in python using PyTorch (Paszke et al., 2019). Several methods rely on an unlabeled validation set to adapt parameters of the anomaly detector, for which we split off 25% of the training set. To tune the hyperparameters of each method, we partition the test set into five folds of roughly equal size, optimize the parameters on each, and evaluate the performance of the best model on the rest. Furthermore, we exclude the folds directly next to the validation fold to mitigate the bias introduced by temporal dependencies. Finally, we report the evaluation averaged over all folds. For our experiments we implemented a sacred-based plugin (Greff et al., 2017) for our library to manage all experiments. We use our fast (linear in time) implementation of $TRec^*$ and $TPrec^*$ to compare all implemented methods using the corresponding $F1$-score[6].

5 Results

We report the main results of our evaluation on SMD and Exathlon in Table 1. We select a reasonable grid of hyperparameters such that we can fully train and evaluate all methods on Exathlon and SMD within two days each[7]. On SMD, we can see a consistently strong performance by older (simpler) methods, such as LSTM-AE (Malhotra et al., 2016) and LSTM-P (Malhotra et al., 2015). In contrast, several modern methods partially seem to perform poorly on SMD (Zhou et al., 2019; Li et al., 2019; Said Elsayed et al., 2020; Hua et al., 2022). We find no method that outperforms its competitors on all datasets. However, the autoencoder- and prediction-based methods seem to be able to perform consistently across multiple datasets and GAN-based methods appear to struggle most among all methods. Methods performing well on SMD generally don't perform well on Exathlon and the other way around.

The variational autoencoder based method GMM-GRU-VAE (Zhang et al., 2021) and the prediction based method GDN (Deng & Hooi, 2021) perform the most consistent across all datasets.

6 Conclusion

Many datasets are severely flawed and form a shaky foundation for AD evaluations. Even carefully constructed datasets (such as those in Exathlon) reveal flaws under careful scrutiny. Despite their well-known problems, point-wise metrics are still the de-facto standard in most evaluations. These (and other) issues create an illusion of progress in time-series AD. We have proposed a general evaluation protocol and a metric that considers temporal dependencies and produces reliable results, as we demonstrate. Evaluating 25 methods in this setting reveals no method that consistently outperforms its competitors. We found that especially modern approaches struggle to reach the performance of older methods.

Our proposed metric is recall consistent and allows for individual bias functions; however, more research on appropriate cardinality functions and their closed-form solutions could reveal new insights. We hope that our comprehensive `TimeSeAD` library helps to shed some light on the progress of (deep) time series AD methods, and further, aids the community to measure the gain of new algorithms in the future.

[6] In Appendix E we provide the complete results, including point-wise metrics and in Appendix D we discuss the evaluation protocol in detail.

[7] We release the full grids alongside the library.

References

Chuadhry Mujeeb Ahmed, Venkata Reddy Palleti, and Aditya P Mathur. Wadi: a water distribution testbed for research in the design of secure cyber physical systems. In *Proceedings of the 3rd international workshop on cyber-physical systems for smart water networks*, pp. 25–28, 2017.

Martin Arjovsky, Soumith Chintala, and Léon Bottou. Wasserstein generative adversarial networks. In Doina Precup and Yee Whye Teh (eds.), *Proceedings of the 34th International Conference on Machine Learning*, volume 70 of *Proceedings of Machine Learning Research*, pp. 214–223. PMLR, 2017. URL `https://proceedings.mlr.press/v70/arjovsky17a.html`.

Julien Audibert, Pietro Michiardi, Frédéric Guyard, Sébastien Marti, and Maria A Zuluaga. Usad: Unsupervised anomaly detection on multivariate time seriesammann2020anomaly. In *Proceedings of the 26th ACM SIGKDD International Conference on Knowledge Discovery & Data Mining*, pp. 3395–3404, 2020.

Julien Audibert, Pietro Michiardi, Frédéric Guyard, Sébastien Marti, and Maria A Zuluaga. Do deep neural networks contribute to multivariate time series anomaly detection? *arXiv preprint arXiv:2204.01637*, 2022.

Aadyot Bhatnagar, Paul Kassianik, Chenghao Liu, Tian Lan, Wenzhuo Yang, Rowan Cassius, Doyen Sahoo, Devansh Arpit, Sri Subramanian, Gerald Woo, et al. Merlion: A machine learning library for time series. *arXiv preprint arXiv:2109.09265*, 2021.

Ane Blázquez-García, Angel Conde, Usue Mori, and Jose A Lozano. A review on outlier/anomaly detection in time series data. *ACM Computing Surveys (CSUR)*, 54(3): 1–33, 2021.

Chris U Carmona, François-Xavier Aubet, Valentin Flunkert, and Jan Gasthaus. Neural contextual anomaly detection for time series. *arXiv preprint arXiv:2107.07702*, 2021.

Cristian I Challu, Peihong Jiang, Ying Nian Wu, and Laurent Callot. Deep generative model with hierarchical latent factors for time series anomaly detection. In *International Conference on Artificial Intelligence and Statistics*, pp. 1643–1654. PMLR, 2022.

Guillaume Chambaret, Laure Berti-Equille, Frédéric Bouchara, Emmanuel Bruno, Vincent Martin, and Fabien Chaillan. Stochastic pairing for contrastive anomaly detection on time series. In *International Conference on Pattern Recognition and Artificial Intelligence*, pp. 306–317. Springer, 2022.

Wenchao Chen, Long Tian, Bo Chen, Liang Dai, Zhibin Duan, and Mingyuan Zhou. Deep variational graph convolutional recurrent network for multivariate time series anomaly detection. In *International Conference on Machine Learning*, pp. 3621–3633. PMLR, 2022.

Zekai Chen, Dingshuo Chen, Xiao Zhang, Zixuan Yuan, and Xiuzhen Cheng. Learning graph structures with transformer for multivariate time series anomaly detection in iot. *IEEE Internet of Things Journal*, 2021.

Kukjin Choi, Jihun Yi, Changhwa Park, and Sungroh Yoon. Deep learning for anomaly detection in time-series data: review, analysis, and guidelines. *IEEE Access*, 2021.

Ailin Deng and Bryan Hooi. Graph neural network-based anomaly detection in multivariate time series. In *Proceedings of the AAAI Conference on Artificial Intelligence*, volume 35, pp. 4027–4035, 2021.

Keval Doshi, Shatha Abudalou, and Yasin Yilmaz. Tisat: Time series anomaly transformer. *arXiv preprint arXiv:2203.05167*, 2022.

Kamil Faber, Marcin Pietron, and Dominik Zurek. Ensemble neuroevolution-based approach for multivariate time series anomaly detection. *Entropy*, 23(11):1466, 2021.

Daniel Fährmann, Naser Damer, Florian Kirchbuchner, and Arjan Kuijper. Lightweight long short-term memory variational auto-encoder for multivariate time series anomaly detection in industrial control systems. *Sensors*, 22(8):2886, 2022.

Pavel Filonov, Andrey Lavrentyev, and Artem Vorontsov. Multivariate industrial time series with cyber-attack simulation: Fault detection using an lstm-based predictive data model. *arXiv preprint arXiv:1612.06676*, 2016.

Astha Garg, Wenyu Zhang, Jules Samaran, Ramasamy Savitha, and Chuan-Sheng Foo. An evaluation of anomaly detection and diagnosis in multivariate time series. *IEEE Transactions on Neural Networks and Learning Systems*, 33(6):2508–2517, 2021.

Alexander Geiger, Dongyu Liu, Sarah Alnegheimish, Alfredo Cuesta-Infante, and Kalyan Veeramachaneni. Tadgan: Time series anomaly detection using generative adversarial networks. In *2020 IEEE International Conference on Big Data (Big Data)*, pp. 33–43. IEEE, 2020.

Jonathan Goh, Sridhar Adepu, Khurum Nazir Junejo, and Aditya Mathur. A dataset to support research in the design of secure water treatment systems. In *International conference on critical information infrastructures security*, pp. 88–99. Springer, 2016.

Klaus Greff, Aaron Klein, Martin Chovanec, Frank Hutter, and Jürgen Schmidhuber. The sacred infrastructure for computational research. In *Proceedings of the 16th python in science conference*, volume 28, pp. 49–56, 2017.

Yifan Guo, Weixian Liao, Qianlong Wang, Lixing Yu, Tianxi Ji, and Pan Li. Multidimensional time series anomaly detection: A gru-based gaussian mixture variational autoencoder approach. In *Asian Conference on Machine Learning*, pp. 97–112. PMLR, 2018.

Yangdong He and Jiabao Zhao. Temporal convolutional networks for anomaly detection in time series. In *Journal of Physics: Conference Series*, volume 1213, pp. 042050. IOP Publishing, 2019.

Hajar Homayouni, Sudipto Ghosh, Indrakshi Ray, Shlok Gondalia, Jerry Duggan, and Michael G Kahn. An autocorrelation-based lstm-autoencoder for anomaly detection on time-series data. In *2020 IEEE International Conference on Big Data (Big Data)*, pp. 5068–5077. IEEE, 2020.

Xiaolei Hua, Lin Zhu, Shenglin Zhang, Zeyan Li, Su Wang, Dong Zhou, Shuo Wang, and Chao Deng. Genad: General representations of multivariate time seriesfor anomaly detection. *arXiv preprint arXiv:2202.04250*, 2022.

Alexis Huet, Jose Manuel Navarro, and Dario Rossi. Local evaluation of time series anomaly detection algorithms. In *Proceedings of the 28th ACM SIGKDD Conference on Knowledge Discovery and Data Mining*, pp. 635–645, 2022.

Kyle Hundman, Valentino Constantinou, Christopher Laporte, Ian Colwell, and Tom Soderstrom. Detecting spacecraft anomalies using lstms and nonparametric dynamic thresholding. In *Proceedings of the 24th ACM SIGKDD international conference on knowledge discovery & data mining*, pp. 387–395, 2018.

Vincent Jacob, Fei Song, Arnaud Stiegler, Bijan Rad, Yanlei Diao, and Nesime Tatbul. Exathlon: A benchmark for explainable anomaly detection over time series. *arXiv preprint arXiv:2010.05073*, 2020.

Wenqian Jiang, Yang Hong, Beitong Zhou, Xin He, and Cheng Cheng. A gan-based anomaly detection approach for imbalanced industrial time series. *IEEE Access*, 7:143608–143619, 2019.

Siwon Kim, Kukjin Choi, Hyun-Soo Choi, Byunghan Lee, and Sungroh Yoon. Towards a rigorous evaluation of time-series anomaly detection. In *Proceedings of the AAAI Conference on Artificial Intelligence*, volume 36, pp. 7194–7201, 2022.

Kwei-Herng Lai, Daochen Zha, Junjie Xu, Yue Zhao, Guanchu Wang, and Xia Hu. Revisiting time series outlier detection: Definitions and benchmarks. In *Thirty-fifth Conference on Neural Information Processing Systems Datasets and Benchmarks Track (Round 1)*, 2021.

Alexander Lavin and Subutai Ahmad. Evaluating real-time anomaly detection algorithms–the numenta anomaly benchmark. In *2015 IEEE 14th international conference on machine learning and applications (ICMLA)*, pp. 38–44. IEEE, 2015.

Chang-Ki Lee, Yu-Jeong Cheon, and Wook-Yeon Hwang. Studies on the gan-based anomaly detection methods for the time series data. *IEEE Access*, 9:73201–73215, 2021.

Dan Li, Dacheng Chen, Jonathan Goh, and See-kiong Ng. Anomaly detection with generative adversarial networks for multivariate time series. *arXiv preprint arXiv:1809.04758*, 2018a.

Dan Li, Dacheng Chen, Baihong Jin, Lei Shi, Jonathan Goh, and See-Kiong Ng. Mad-gan: Multivariate anomaly detection for time series data with generative adversarial networks. In *International Conference on Artificial Neural Networks*, pp. 703–716. Springer, 2019.

Longyuan Li, Junchi Yan, Haiyang Wang, and Yaohui Jin. Anomaly detection of time series with smoothness-inducing sequential variational auto-encoder, 2021a.

Yaguang Li, Rose Yu, Cyrus Shahabi, and Yan Liu. Diffusion convolutional recurrent neural network: Data-driven traffic forecasting. In *International Conference on Learning Representations*, 2018b. URL https://openreview.net/forum?id=SJiHXGWAZ.

Zhihan Li, Youjian Zhao, Jiaqi Han, Ya Su, Rui Jiao, Xidao Wen, and Dan Pei. Multivariate time series anomaly detection and interpretation using hierarchical inter-metric and temporal embedding. In *Proceedings of the 27th ACM SIGKDD Conference on Knowledge Discovery & Data Mining*, pp. 3220–3230, 2021b.

Benjamin Lindemann, Benjamin Maschler, Nada Sahlab, and Michael Weyrich. A survey on anomaly detection for technical systems using lstm networks. *Computers in Industry*, 131:103498, 2021.

Yuan Luo, Ya Xiao, Long Cheng, Guojun Peng, and Danfeng Yao. Deep learning-based anomaly detection in cyber-physical systems: Progress and opportunities. *ACM Computing Surveys (CSUR)*, 54(5):1–36, 2021.

Pankaj Malhotra, Lovekesh Vig, Gautam Shroff, and Puneet Agarwal. Long short term memory networks for anomaly detection in time series. In *23rd European Symposium on Artificial Neural Networks, ESANN 2015, Bruges, Belgium, April 22-24, 2015*, 2015. URL http://www.elen.ucl.ac.be/Proceedings/esann/esannpdf/es2015-56.pdf.

Pankaj Malhotra, Anusha Ramakrishnan, Gaurangi Anand, Lovekesh Vig, Puneet Agarwal, and Gautam Shroff. Lstm-based encoder-decoder for multi-sensor anomaly detection. *arXiv preprint arXiv:1607.00148*, 2016.

Ali H Mirza and Selin Cosan. Computer network intrusion detection using sequential lstm neural networks autoencoders. In *2018 26th signal processing and communications applications conference (SIU)*, pp. 1–4. IEEE, 2018.

Mohsin Munir, Shoaib Ahmed Siddiqui, Andreas Dengel, and Sheraz Ahmed. Deepant: A deep learning approach for unsupervised anomaly detection in time series. *Ieee Access*, 7: 1991–2005, 2018.

Zijian Niu, Ke Yu, and Xiaofei Wu. Lstm-based vae-gan for time-series anomaly detection. *Sensors*, 20(13):3738, 2020.

Daehyung Park, Yuuna Hoshi, and Charles C Kemp. A multimodal anomaly detector for robot-assisted feeding using an lstm-based variational autoencoder. *IEEE Robotics and Automation Letters*, 3(3):1544–1551, 2018.

Adam Paszke, Sam Gross, Francisco Massa, Adam Lerer, James Bradbury, Gregory Chanan, Trevor Killeen, Zeming Lin, Natalia Gimelshein, Luca Antiga, et al. Pytorch: An imperative style, high-performance deep learning library. *Advances in neural information processing systems*, 32, 2019.

Joao Pereira and Margarida Silveira. Unsupervised anomaly detection in energy time series data using variational recurrent autoencoders with attention. In *2018 17th IEEE international conference on machine learning and applications (ICMLA)*, pp. 1275–1282. IEEE, 2018.

Danilo Rezende and Shakir Mohamed. Variational inference with normalizing flows. In Francis Bach and David Blei (eds.), *Proceedings of the 32nd International Conference on Machine Learning*, volume 37 of *Proceedings of Machine Learning Research*, pp. 1530–1538, Lille, France, 2015. PMLR. URL `https://proceedings.mlr.press/v37/rezende15.html`.

Lukas Ruff, Jacob R. Kauffmann, Robert A. Vandermeulen, Grégoire Montavon, Wojciech Samek, Marius Kloft, Thomas G. Dietterich, and Klaus-Robert Müller. A unifying review of deep and shallow anomaly detection. *Proc. IEEE*, 109(5):756–795, 2021.

Mahmoud Said Elsayed, Nhien-An Le-Khac, Soumyabrata Dev, and Anca Delia Jurcut. Network anomaly detection using lstm based autoencoder. In *Proceedings of the 16th ACM Symposium on QoS and Security for Wireless and Mobile Networks*, pp. 37–45, 2020.

Erik Scharwächter and Emmanuel Müller. Statistical evaluation of anomaly detectors for sequences. *arXiv preprint arXiv:2008.05788*, 2020.

Sebastian Schmidl, Phillip Wenig, and Thorsten Papenbrock. Anomaly detection in time series: a comprehensive evaluation. *Proceedings of the VLDB Endowment*, 15(9):1779–1797, 2022.

Bernhard Schölkopf, John C. Platt, John Shawe-Taylor, Alex J. Smola, and Robert C. Williamson. Estimating the Support of a High-Dimensional Distribution. *Neural Computation*, 13(7):1443–1471, 07 2001. ISSN 0899-7667. doi: 10.1162/089976601750264965. URL `https://doi.org/10.1162/089976601750264965`.

Lifeng Shen, Zhuocong Li, and James Kwok. Timeseries anomaly detection using temporal hierarchical one-class network. *Advances in Neural Information Processing Systems*, 33: 13016–13026, 2020.

Maximilian Sölch, Justin Bayer, Marvin Ludersdorfer, and Patrick van der Smagt. Variational inference for on-line anomaly detection in high-dimensional time series. *arXiv preprint arXiv:1602.07109*, 2016.

Ya Su, Youjian Zhao, Chenhao Niu, Rong Liu, Wei Sun, and Dan Pei. Robust anomaly detection for multivariate time series through stochastic recurrent neural network. In *Proceedings of the 25th ACM SIGKDD International Conference on Knowledge Discovery & Data Mining*, pp. 2828–2837, 2019.

Nesime Tatbul, Tae Jun Lee, Stan Zdonik, Mejbah Alam, and Justin Gottschlich. Precision and recall for time series. *Advances in neural information processing systems*, 31, 2018.

Markus Thill, Wolfgang Konen, and Thomas Bäck. Time series encodings with temporal convolutional networks. In *International Conference on Bioinspired Methods and Their Applications*, pp. 161–173. Springer, 2020.

Petar Veličković, Guillem Cucurull, Arantxa Casanova, Adriana Romero, Pietro Liò, and Yoshua Bengio. Graph attention networks. In *International Conference on Learning Representations*, 2018. URL `https://openreview.net/forum?id=rJXMpikCZ`.

Taras K. Vintsyuk. Speech discrimination by dynamic programming. *Cybernetics*, 4(1): 52–57, January 1968. ISSN 1573-8337. doi: 10.1007/BF01074755. URL `https://doi.org/10.1007/BF01074755`.

Lan Wang, Yusan Lin, Yuhang Wu, Huiyuan Chen, Fei Wang, and Hao Yang. Forecast-based multi-aspect framework for multivariate time-series anomaly detection. In *2021 IEEE International Conference on Big Data (Big Data)*, pp. 938–947. IEEE, 2021.

Qingsong Wen, Tian Zhou, Chaoli Zhang, Weiqi Chen, Ziqing Ma, Junchi Yan, and Liang Sun. Transformers in time series: A survey. *arXiv preprint arXiv:2202.07125*, 2022.

Renjie Wu and Eamonn Keogh. Current time series anomaly detection benchmarks are flawed and are creating the illusion of progress. *IEEE Transactions on Knowledge and Data Engineering*, 2021.

Qinfeng Xiao, Shikuan Shao, and Jing Wang. Memory-augmented adversarial autoencoders for multivariate time-series anomaly detection with deep reconstruction and prediction. *arXiv preprint arXiv:2110.08306*, 2021.

Haowen Xu, Yang Feng, Jie Chen, Zhaogang Wang, Honglin Qiao, Wenxiao Chen, Nengwen Zhao, Zeyan Li, Jiahao Bu, Zhihan Li, and et al. Unsupervised anomaly detection via variational auto-encoder for seasonal kpis in web applications. *Proceedings of the 2018 World Wide Web Conference on World Wide Web - WWW '18*, 2018. doi: 10.1145/3178876.3185996. URL `http://dx.doi.org/10.1145/3178876.3185996`.

Jiehui Xu, Haixu Wu, Jianmin Wang, and Mingsheng Long. Anomaly transformer: Time series anomaly detection with association discrepancy. *arXiv preprint arXiv:2110.02642*, 2021.

Jun Zhan, Siqi Wang, Xiandong Ma, Chengkun Wu, Canqun Yang, Detian Zeng, and Shilin Wang. Stgat-mad: Spatial-temporal graph attention network for multivariate time series anomaly detection. In *ICASSP 2022-2022 IEEE International Conference on Acoustics, Speech and Signal Processing (ICASSP)*, pp. 3568–3572. IEEE, 2022.

Chuxu Zhang, Dongjin Song, Yuncong Chen, Xinyang Feng, Cristian Lumezanu, Wei Cheng, Jingchao Ni, Bo Zong, Haifeng Chen, and Nitesh V Chawla. A deep neural network for unsupervised anomaly detection and diagnosis in multivariate time series data. In *Proceedings of the AAAI conference on artificial intelligence*, volume 33, pp. 1409–1416, 2019.

Hongjing Zhang, Fangzhou Cheng, and Aparna Pandey. One-class predictive autoencoder towards unsupervised anomaly detection on industrial time series. In *ANDEA '22*, 2022a.

Kai Zhang, Yushan Jiang, Lee Seversky, Chengtao Xu, Dahai Liu, and Houbing Song. Federated variational learning for anomaly detection in multivariate time series. In *2021 IEEE International Performance, Computing, and Communications Conference (IPCCC)*, pp. 1–9. IEEE, 2021.

Weiqi Zhang, Chen Zhang, and Fugee Tsung. Grelen: Multivariate time series anomaly detection from the perspective of graph relational learning. In Lud De Raedt (ed.), *Proceedings of the Thirty-First International Joint Conference on Artificial Intelligence, IJCAI-22*, pp. 2390–2397. International Joint Conferences on Artificial Intelligence Organization, 7 2022b. doi: 10.24963/ijcai.2022/332. Main Track.

Hang Zhao, Yujing Wang, Juanyong Duan, Congrui Huang, Defu Cao, Yunhai Tong, Bixiong Xu, Jing Bai, Jie Tong, and Qi Zhang. Multivariate time-series anomaly detection via graph attention network. In *2020 IEEE International Conference on Data Mining (ICDM)*, pp. 841–850. IEEE, 2020.

Bin Zhou, Shenghua Liu, Bryan Hooi, Xueqi Cheng, and Jing Ye. Beatgan: Anomalous rhythm detection using adversarially generated time series. In *IJCAI*, pp. 4433–4439, 2019.

A Metrics

Let $X \in \mathbb{R}^{T\times F}$ be a time series of length T and dimension F and let $y \in \mathbb{R}^T$ the corresponding labels. Given an online anomaly detector $s\colon \mathbb{R}^{T\times F} \to \mathbb{R}^T$ that computes a score for each time step in X based only on points that came before it. The set of anomalies is

$$\mathcal{A} = \{[a,b] \subset [T] \mid \forall t \in [a,b]\colon y[t] = 1; \nexists [a',b'] \supsetneq [a,b]\colon \forall t \in [a',b']\colon y[t] = 1\}$$

and the set of all predictions for a threshold $\lambda \in \mathbb{R}$ is

$$\mathcal{P}^\lambda = \{[a,b] \subset [T] \mid \forall t \in [a,b]\colon s(x)[t] \geq \lambda; \nexists [a',b'] \supsetneq [a,b]\colon \forall t \in [a',b']\colon s(x)[t] \geq \lambda\}.$$

Given a cardinality function $\gamma\colon \mathbb{N} \times \mathcal{P}([T]) \to \mathbb{R}_{\geq 0}$ and a bias function $\delta\colon \mathbb{R} \to \mathbb{R}_{\geq 0}$, time-series recall is given by

$$TRec(\mathcal{A},\mathcal{P}) = \frac{1}{|\mathcal{A}|}\sum_{A\in\mathcal{A}}\left[\alpha\mathbb{1}(|\mathcal{P}_A|>0) + (1-\alpha)\gamma(|\mathcal{P}_A|,A)\sum_{P\in\mathcal{P}}\frac{\sum_{t\in P\cap A}\delta(t-\min A,|A|)}{\sum_{t\in A}\delta(t-\min A,|A|)}\right]$$

with $\mathcal{P}_A = \{P \in P \mid |A \cap P| > 0\}$. The cardinality function is monotone decreasing in its first argument and $\gamma(1,\cdot) = 1$.

Proof of Theorem 1: It is straight-forward to see, that γ is monotone decreasing, as the maximum is over all values with smaller inputs multiplied by a factor smaller than one. It remains to show, that the resulting $TRec$ is recall consistent.

Since the terms within the sum are all non-negative, it suffices show, that each individual term only ever decreases. Consider two thresholds $\lambda, \lambda' \in \mathbb{R}$ with $\lambda' > \lambda$ and anomaly $A \in \mathcal{A}$ such that $\mathcal{P}_A^\lambda \neq \mathcal{P}_A^{\lambda'}$. Note that $|\mathcal{P}_A^\lambda| = 0$ implies $|\mathcal{P}_A^{\lambda'}| = 0$. If $|\mathcal{P}_A^{\lambda'}| = 0$ the inner sum is zero and the statement is true. Thus, we assume $|\mathcal{P}_A^{\lambda'}| > 0$ and can therefore ignore the first term inside the outer sum, since $\mathbb{1}(|\mathcal{P}_A^\lambda| > 0) = \mathbb{1}(|\mathcal{P}_A^{\lambda'}| > 0)$ always holds.

First, we consider the case $|\mathcal{P}_A^{\lambda'}| \geq |\mathcal{P}_A^\lambda|$. Since γ is monotone decreasing in its first argument and the inner sum looses at least one non-negative term, the second term can either decrease or stay the same.

Next, we consider the case $|\mathcal{P}_A^{\lambda'}| < |\mathcal{P}_A^\lambda|$. We want to show, that each term only ever decreases with an increasing threshold, i.e.

$$\gamma(|\mathcal{P}_A^\lambda|,A)\sum_{P\in\mathcal{P}_A^\lambda}\frac{\sum_{t\in P\cap A}\delta(t-\min A,|A|)}{\sum_{t\in A}\delta(t-\min A,|A|)} \geq \gamma(|\mathcal{P}_A^{\lambda'}|,A)\sum_{P\in\mathcal{P}_A^{\lambda'}}\frac{\sum_{t\in P\cap A}\delta(t-\min A,|A|)}{\sum_{t\in A}\delta(t-\min A,|A|)}.$$

If $\gamma(|\mathcal{P}_A^{\lambda'}|, A) = 0$, the recall does not not change, because γ is monotone decreasing. Thus we assume $\gamma(|\mathcal{P}_A^{\lambda'}|, A) > 0$, in which case the inequality above holds if and only if

$$\frac{\gamma(|\mathcal{P}_A^\lambda|,A)}{\gamma(|\mathcal{P}_A^{\lambda'}|,A)} \geq \frac{\sum_{P\in\mathcal{P}_A^{\lambda'}}\sum_{t\in P\cap A}\delta(t-\min A,|A|)}{\sum_{P\in\mathcal{P}_A^{\lambda}}\sum_{t\in P\cap A}\delta(t-\min A,|A|)}.$$

Consider $\Delta\delta = \sum_{P\in\mathcal{P}_A^\lambda}\sum_{t\in P\cap A}\delta(t-\min A,|A|) - \sum_{P\in\mathcal{P}_A^{\lambda'}}\sum_{t\in P\cap A}\delta(t-\min A,|A|) > 0$. Then it holds

$$\Delta\delta \geq |\bigcup_{\substack{P\in\mathcal{P}_A^\lambda \\ P'\in\mathcal{P}_A^{\lambda'}}} P \setminus P'| \geq |\mathcal{P}_A^\lambda| - |\mathcal{P}_A^{\lambda'}|$$

Since $P \cap A \subset A$, we also know

$$\frac{\sum_{P \in \mathcal{P}_A^{\lambda'}} \sum_{t \in P \cap A} \delta(t - \min A, |A|)}{\sum_{P \in \mathcal{P}_A^{\lambda}} \sum_{t \in P \cap A} \delta(t - \min A, |A|)} = \frac{\sum_{P \in \mathcal{P}_A^{\lambda}} \sum_{t \in P \cap A} \delta(t - \min A, |A|) - \Delta\delta}{\sum_{P \in \mathcal{P}_A^{\lambda}} \sum_{t \in P \cap A} \delta(t - \min A, |A|)}$$
$$\leq \frac{\sum_{t \in A} \delta(t - \min A, |A|) - \Delta\delta}{\sum_{t \in A} \delta(t - \min A, |A|)}$$
$$\leq \frac{\sum_{t \in A} \delta(t - \min A, |A|) - (|\mathcal{P}_A^{\lambda}| - |\mathcal{P}_A^{\lambda'}|)}{\sum_{t \in A} \delta(t - \min A, |A|)}$$

Thus, if

$$\gamma(|\mathcal{P}_A^{\lambda}|, A) \geq \frac{\sum_{t \in A} \delta(t - \min A, |A|) - (|\mathcal{P}_A^{\lambda}| - |\mathcal{P}_A^{\lambda'}|)}{\sum_{t \in A} \delta(t - \min A, |A|)} \gamma(|\mathcal{P}_A^{\lambda'}|, A)$$

holds true for all $0 < |\mathcal{P}_A^{\lambda'}| < |\mathcal{P}_A^{\lambda}|$, the resulting recall is recall consistent. □

Lemma 1 For any $x \in \mathbb{R}_{\geq 1}$ it holds $\left(\frac{x-1}{x}\right)^n \geq \frac{x-n}{x}$ for all $n \in \mathbb{N}$.
Proof: We know $\left(\frac{x-1}{x}\right)^1 = \frac{x-1}{x}$. By induction over n it holds

$$\left(\frac{x-1}{x}\right)^{n+1} \geq \frac{x-1}{x}\frac{x-n}{x} = \frac{x-(n+1)}{x} + \frac{n}{x^2} \geq \frac{x-(n+1)}{x}$$

□

B Datasets

In this section we provide a more detailed description and analysis of all considered datasets. Additionally we provide further examples of any issues we found. First and foremost, we provide the general statistics of each datasets, see Table 2.

Table 2: Statistics of each dataset

Dataset	Features	train size	test size	Anomalies	
SWaT	51	495000	449919	35	12.1%
WADI	123	784571	172801	14	5.8%
SMAP	25	140825	444035	69	12.8%
MSL	55	58317	73729	36	10.5%
SMD 0	38	28479	28479	8	9.5 %
SMD 1	38	23694	23694	10	2.3 %
SMD 2	38	23702	23703	12	3.4 %
SMD 3	38	23706	23707	12	3.0 %
SMD 4	38	23705	23706	7	0.4 %
SMD 5	38	23688	23689	30	15.7 %
SMD 6	38	23697	23697	13	10.1 %
SMD 7	38	23698	23699	20	3.2 %
SMD 8	38	23693	23694	13	4.9 %
SMD 9	38	23699	23700	11	12.0 %
SMD 10	38	23688	23689	10	1.1 %
SMD 11	38	23689	23689	20	7.2 %
SMD 12	38	23688	23689	21	4.1 %
SMD 13	38	28743	28743	8	1.5 %
SMD 14	38	23696	23696	20	1.8 %
SMD 15	38	23702	23703	1	0.7 %
SMD 16	38	28722	28722	10	6.1 %
SMD 17	38	28700	28700	4	1.1 %
SMD 18	38	23692	23693	13	4.4 %
SMD 19	38	28695	28696	3	0.7 %
SMD 20	38	23702	23703	10	4.7 %
SMD 21	38	23703	23703	26	2.7 %
SMD 22	38	23687	23687	8	4.1 %
SMD 23	38	23690	23691	11	1.8 %
SMD 24	38	28726	28726	11	4.2 %
SMD 25	38	28705	28705	5	1.5 %
SMD 26	38	28703	28704	6	4.8 %
SMD 27	38	28713	28713	4	1.1 %
Exathlon 1	19	41382	49810	9	17.1 %
Exathlon 2	19	68917	96535	9	17.6 %
Exathlon 3	19	115160	15270	7	16.0 %
Exathlon 4	19	208720	133223	11	12.6 %
Exathlon 5	19	133411	190372	21	9.5 %
Exathlon 6	19	303087	97221	11	9.6 %
Exathlon 9	19	273247	103511	14	13.0 %
Exathlon 10	19	178685	106251	13	13.9 %

Papers that evaluate on SWaT include (Li et al., 2018a; 2019; Audibert et al., 2020; Shen et al., 2020; Faber et al., 2021; Zhang et al., 2021; Xiao et al., 2021; Deng & Hooi, 2021; Carmona et al., 2021; Xu et al., 2021; Li et al., 2021b; Fährmann et al., 2022; Doshi et al., 2022; Zhan et al., 2022; Zhang et al., 2022b;a).

Papers that evaluate on WADI include (Li et al., 2019; Audibert et al., 2020; Faber et al., 2021; Deng & Hooi, 2021; Xu et al., 2021; Li et al., 2021b; Fährmann et al., 2022; Zhan et al., 2022; Zhang et al., 2022b;a).

Papers that evaluate on SMAP include (Hundman et al., 2018; Audibert et al., 2020; Geiger et al., 2020; Zhao et al., 2020; Shen et al., 2020; Zhang et al., 2021; Xiao et al., 2021; Carmona et al., 2021; Xu et al., 2021; Challu et al., 2022; Chen et al., 2022; Doshi et al., 2022; Hua et al., 2022; Chambaret et al., 2022; Zhang et al., 2022a)

Papers that evaluate on MSL include (Hundman et al., 2018; Su et al., 2019; Audibert et al., 2020; Geiger et al., 2020; Zhao et al., 2020; Shen et al., 2020; Zhang et al., 2021; Xiao et al., 2021; Wang et al., 2021; Xu et al., 2021; Challu et al., 2022; Chen et al., 2022; Doshi et al., 2022; Hua et al., 2022; Chambaret et al., 2022; Zhang et al., 2022a)

Papers that evaluate on SMD include (Su et al., 2019; Audibert et al., 2020; Xiao et al., 2021; Wang et al., 2021; Carmona et al., 2021; Xu et al., 2021; Li et al., 2021b; Challu et al., 2022; Chen et al., 2022; Doshi et al., 2022; Hua et al., 2022; Zhan et al., 2022; Zhang et al., 2022b)

Papers that evaluate on Exathlon include (Schmidl et al., 2022).

B.1 Secure Water Treatement (SWaT)

The Secure Water Treatment (SWaT) dataset Goh et al. (2016) originates from the operation of a miniature water-treatment plant. 51 sensors were recorded during 11 days of plant operation at a sampling rate of 1 Hz. The dataset is split into a training set and a test set. The training set corresponds to the first six days of operation, during which no incidents occurred. The remaining five days make up the test set. During this time, 36 attacks on the miniature plant were conducted, both against the plant's physical components and its control software. A time step is labeled anomalous, if an attack occurred at that time. In total, Goh et al. (2016) conducted 36 attacks against the system, of which two overlap, so they make up a single anomaly window. The average attack length is around 600 time steps (10minutes). Goh et al. (2016) note that the data recording started when the plant was offline, and the first 5 hours correspond to the plant's start-up procedure. They have already removed the first 30 minutes from the dataset, but we follow Li et al. (2019) and remove the 4.5 hours after that as well. Otherwise, those data points could hamper some methods attempting to model the distribution or process that generates normal data.

With roughly 12% of points anomalous, SWaT's anomaly density is barely acceptable. The distribution of anomaly positions in SWaT, see Figure 6a, reveals no clear bias, except for one large cluster in the middle of the time-series. Looking at the lengths of anomaly

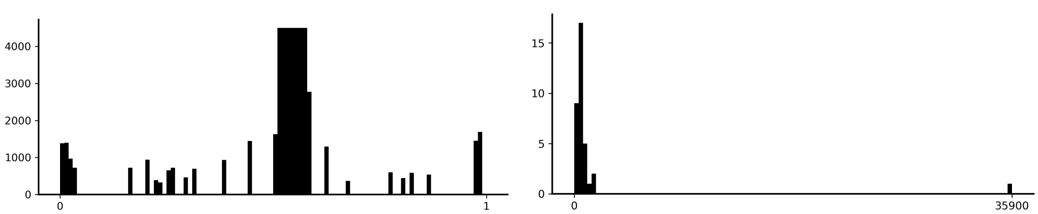

(a) Relative anomaly positions

(b) Anomaly window lengths

Figure 6: Relative position of anomalies (a) and the distribution of anomaly lengths (b) in the test set of SWaT.

windows, see Figure 6b reveals an extremely long anomaly window containing more than 35,000 points (8.5 hours). This lengths by far exceeds any reasonable setting for window sizes, which usually are smaller than 100.

Looking at the mean and standard deviation of the features in SWaT, see Figure 7, reveals clear instances of distributional shift, some features that are constant throughout training and test set, and several features that seem trivial to solve. The consistently constant features mostly correspond to backup actuators that only become active when their primary counterpart fails for some reason. As this does not occur during the training period, the backup actuators never activate. We test a trivial thresholding method on each feature, by using the distance to the mean computed from the training set as anomaly score. Indeed,

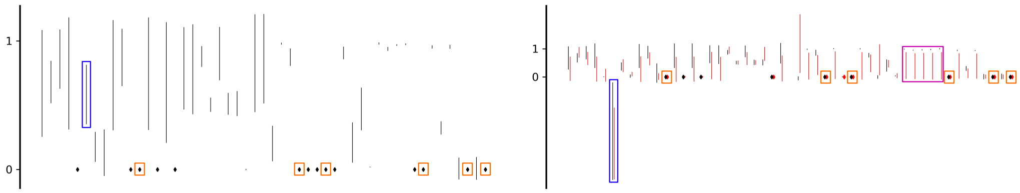

(a) Train set feature distribution (b) Test set feature distribution

Figure 7: Mean and standard deviation for each feature in SWaT of normal points (black) and anomalies (red). Multiple features are constant across the entire dataset (diamond), some even across training and test set (orange box). Other features suggest a distributional shift between training and test set (blue box). Some features appear almost trivial in the test set (purple box).

for several features, we can achieve comparable performance to several deep methods. However, many modern methods still outperform the trivial baseline. Inspecting the features in question reveals one large anomaly responsible for the deviating mean. Multiple smaller anomalies, however, are not trivially reflected in the feature alone, see Figure 8. The specification reveals, that these sensors are flow meters. Even though a thresholding method on these features presents a strong baseline, especially with respect to point-wise metrics, these features do not seem trivial.

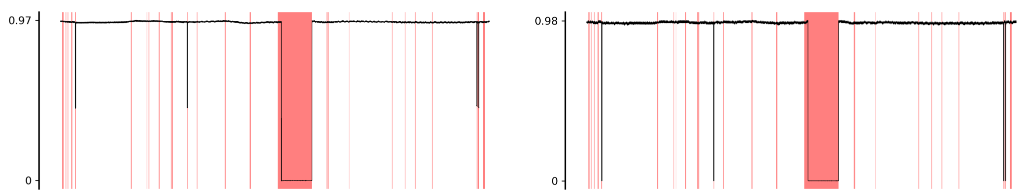

(a) FIT503 (b) FIT504

Figure 8: Two features from the test set of SWaT.

Looking at other features in SWaT, reveals some instances, where anomalies seem to cause late- or long-term effects, see Figure 9. In on instance (Figure 9b), the behaviour of a feature drastically changes after some anomalies have occured, causing a severe distributional shift in that feature. Another example shows a sudden abnormal spike shortly after an anomaly window. Since such sikes or distributional shift does not appear in the training set, it does not seem reasonable for a fully trained anomaly detection algorithm to ignore such instances.

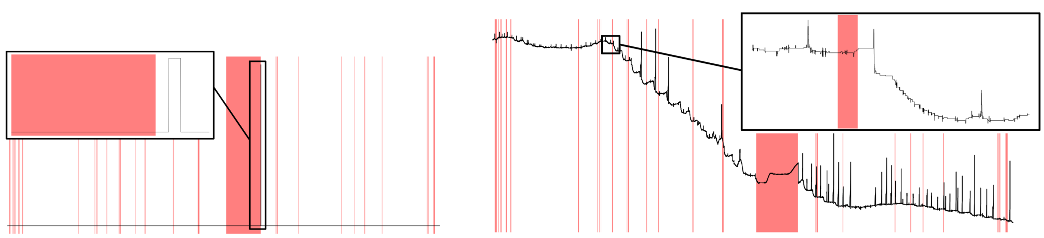

(a) P403 (b) AIT201

Figure 9: Two features from the test set of SWaT. Each feature was normalized based on the statistics of the training-set.

B.2 **WA**TER **DI**STRIBUTION (WADI)

The Water Distribution (WADI) (Ahmed et al., 2017) dataset is similar to SWaT. Its 123 features correspond to sensor values/actuator states in a miniature water-distribution grid connected to the SWaT water-treatment plant. Ahmed et al. (2017) recorded the operation of the grid for 16 continuous days at a sample rate of 1 Hz and launched a total of 15 attacks in the last two days. Thus, the test set is a single time series corresponding to the last two days of operation, whereas the training set consists of the first 14 days. We use version A2 of the dataset, where the authors removed a good chunk of the original data (425,030 of 1,209,601 data points) from the middle of the training set, which is therefore now split into two TS. Note that the dataset file actually contains 127 columns. However, 4 of those do not contain any value at any time step, so we remove them entirely. There are also some spurious missing values in the remaining data, which we simply replace with the last available value for the affected feature.

The anomaly density in WADI seems reasonable with 6% and the anomalies seem reasonably distributed, even if they are mostely clustered at the beginning, end, and middle of the time series, see Figure 10a. There is now extermely long anomaly window such as in SWaT.

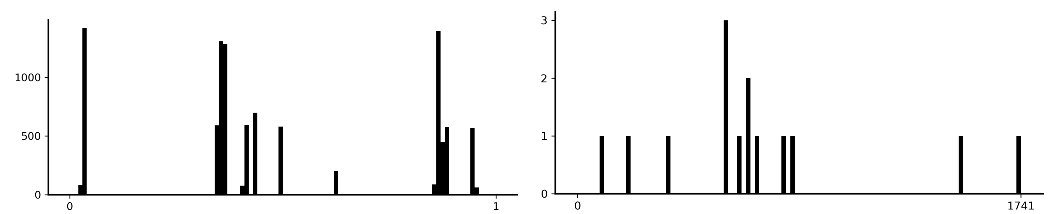

(a) Relative anomaly positions

(b) Anomaly window lengths

Figure 10: Relative position of anomalies (a) and the distribution of anomaly lengths (b) in the test set of WADI.

However, several windows contain over 1,000 points, which we sould still consider too long in general. Looking at the feature distribution, see Figure 11, we can see one feature in particular, for which the distributions vastly differ. Examining the piping diagram of WADI

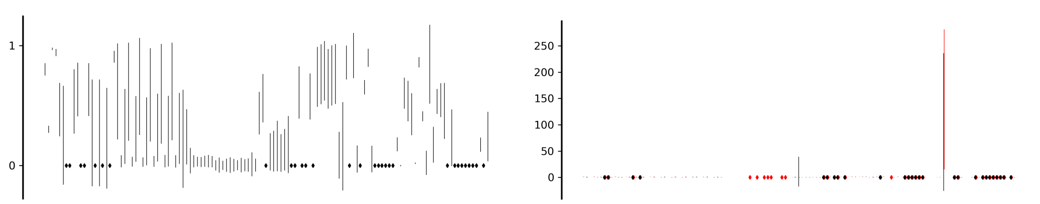

(a) Train set feature distribution

(b) Test set feature distribution

Figure 11: Mean and standard deviation for each feature in SWaT of normal points (black) and anomalies (red). Multiple features are constant across the entire dataset (diamond).

reveals that the exploding feature belongs to a turbidity sensor, and the authors claim that the previous attack introduces contaminated water to the grid. Therefore, it is not unlikely that the attack was the cause for the explosion of that feature. We are no experts on the subject, but the sensor data jumps to about 200 after normalization, see Figure 12b. If this is intended behaviour, there is no way to infer this based on the training set. In other sensors we can observe possible late effects as well, see Figure 12a.

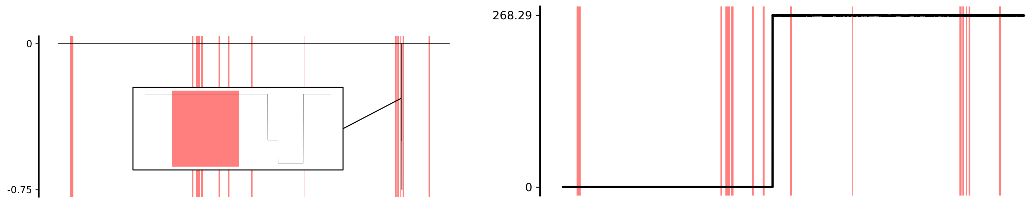

(a) 2_P_004_SPEED (b) 2A_AIT_002_PV

Figure 12: Two features from the test set of WADI. Each feature was normalized based on the statistics of the training-set.

B.3 Soil Moisture Active Passive (SMAP)

The Soil Moisture Active Passive dataset (Hundman et al., 2018) contains 55 time series. All but one feature in each time series correspond to commands sent to a satellite at a given point in time and are represented by binary features. The remaining feature contains the actual sensor values reported by the satellite. Each time series corresponds to a possibly different telemetry channel of that satellite. Thus, at least one feature is different for all time series. Furthermore, we were not able to find a specification of the remaining features. Thus, we have no way of verifying their consistency across different time series. All things considered, the time series in SMAP are technically generated by different processes and should be treated as such. To illustrate the extent of the differences between individual time series, we visualize the sensor feature from multiple time series in the training set, see Figure 13.

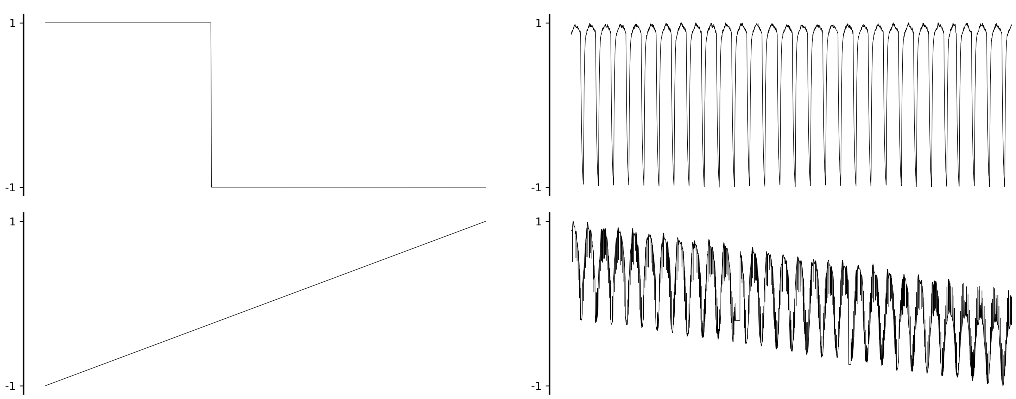

Figure 13: The sensor feature from different time series in the training set of SMAP.

Beyond the conceptual flaws, we still find a clear positional bias towards the latter half of the time series, see Figure 14a, and several anomalies longer than 2000 time points, see Figure 14b.

Since the time series are generated by different processes, we examine the distributional changes within each time series. We find instances, where all command features are constant throughout the test time series or at least after some initial period, see Figure 15. Since all methods rely on windowing, the sensor feature provides the only context for prediction, see Figure 16. Since the feature is constant before and after the anomaly and no additional information is provided by the command features, this does not seem to be reasonable task for anomaly detection. The example shows an instance, where anomalies seem to cause long-term effects, which are not reflected in the label. We can find more examples of this behaviour throughout the dataset, see Figure 17.

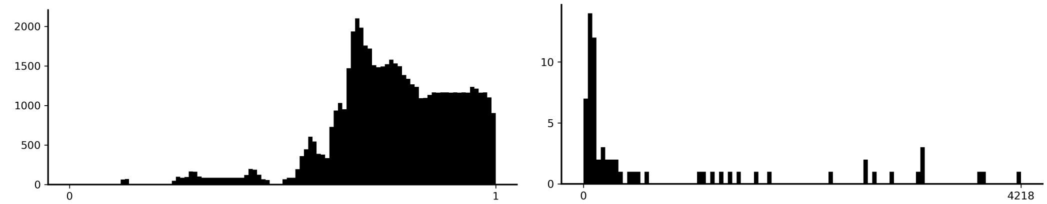

(a) Relative anomaly positions

(b) Anomaly window lengths

Figure 14: Relative position of anomalies (a) and the distribution of anomaly lengths (b) in the test set of SMAP.

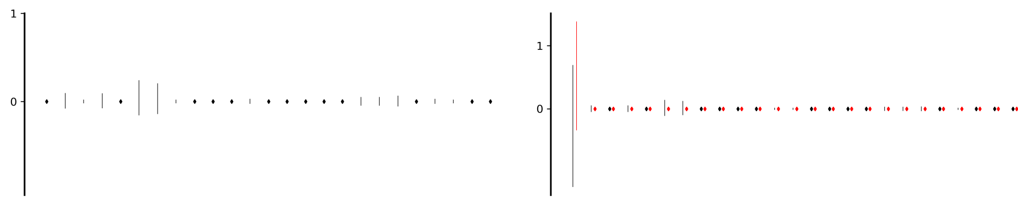

(a) Train set feature distribution

(b) Test set feature distribution

Figure 15: Example of the feature means and standard deviations

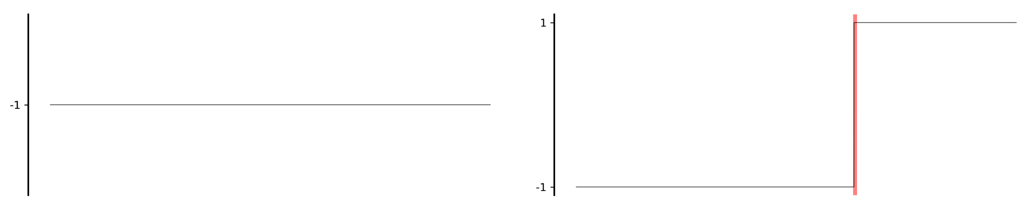

(a) Sensor in training set

(b) Sensor in test set

Figure 16: Example of the sensor feature in training and test set.

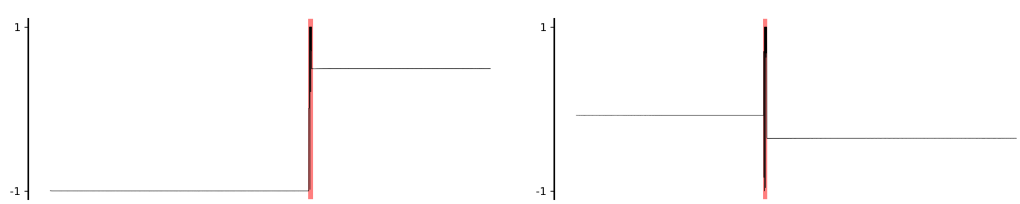

Figure 17: Example of distributional shift in the sensor feature in the test set of SMAP.

B.4 Mars Science Lab (MSL)

The Mars Sience Lab dataset (Hundman et al., 2018) is similarly constructed as SMAP. It contains 27 time series, each containing a single telemetry value feature and binary encoded command for the rest. Thus, it shares many of the same problems as SMAP, see Figure 18.

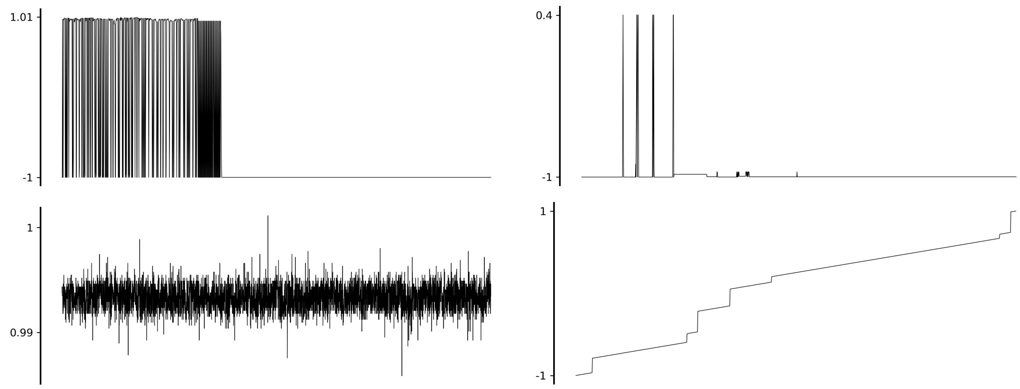

Figure 18: The sensor feature from different time series in the training set of MSL.

The positional bias, see Figure 19a, and long anomalies, see Figure 19b, are not as pronounced as in SMAP, but still noticable.

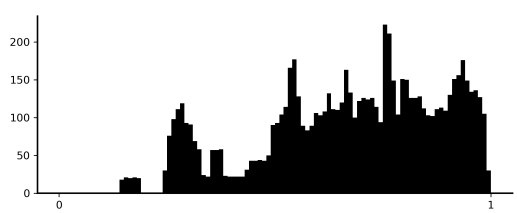

(a) Relative anomaly positions

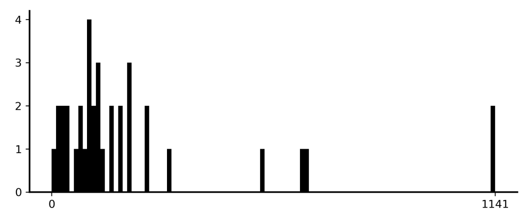

(b) Anomaly window lengths

Figure 19: Relative position of anomalies (a) and the distribution of anomaly lengths (b) in the test set of SMAP.

Similarly to SMAP, we can identify instances of possible distributional shift and long-term effects, see Figure 20.

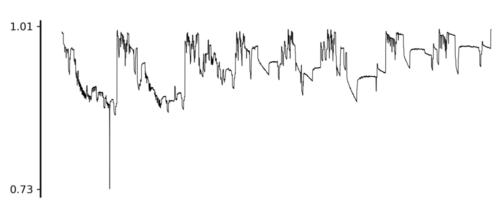

(a) Sensor in training set

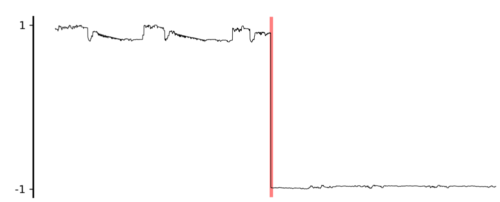

(b) Sensor in test set

Figure 20: Example of the sensor feature in training and test set of MSL. In a wide window around the anomaly window all other features are constant.

Taking all these issues together, both SMAP and MSL do not seem suited for the evaluation of general deep time-series AD. Specialized methods that exploit the intricacies of the data will most likely outperform any general algorithms. Because the datasets are lacking a detailed documentation it is difficult to assess the extent to which the long-term effects seemingly caused by anomalies are intended behavior. Even then, the datasets might be more suited to change point detection methods. Since the command features are constant for a large portion of both datasets, it begs the question how much they can contribute for general algorithms and if the problem is as complex as their presence suggests.

B.5 Server Machine Data (SMD)

The Server Machine Data dataset (Su et al., 2019) consists of 28 time series. According to the authors, the dataset was collected from a large internet company over a period of five weeks. The first half of the dataset comprises the training set and the latter half the test set. Unfortunately we were not able to find any more information on this dataset. However, because each time series was apparently sampled under different conditions, each time series in this dataset should be considered independently.

Looking at the distribution of anomaly positions in each time series, we can identify three instances with clear positional bias towards the end of the time series, see Figure 21a top. For one server in particular, see Figure 21 middle, the distribution is dominated by one large anomaly. For most time series, however, anomaly windows never exceed 1,000 time steps

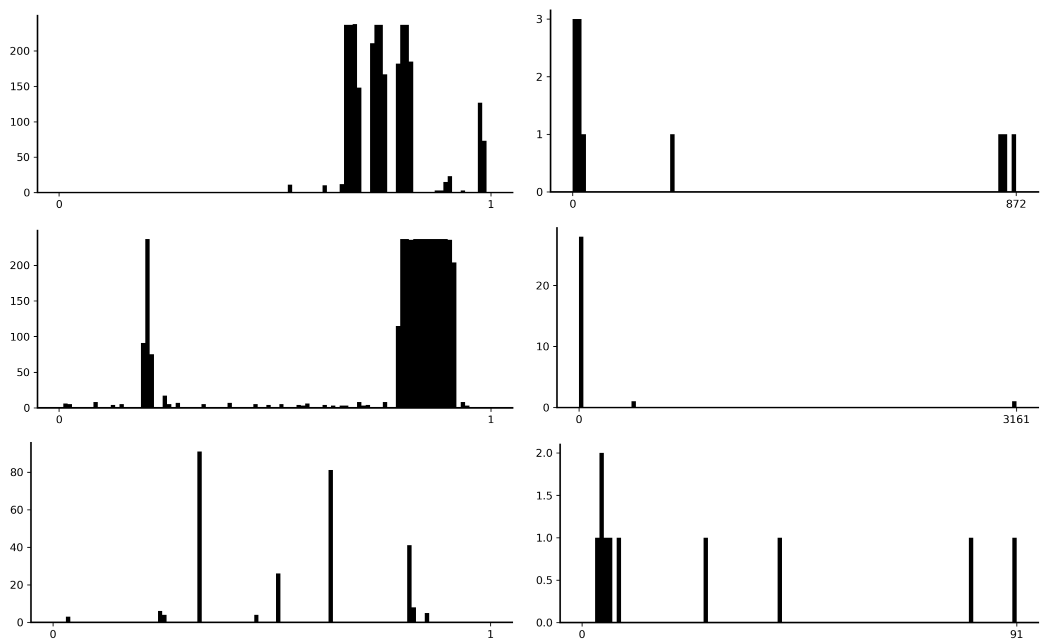

(a) Relative anomaly positions (b) Anomaly window lengths

Figure 21: Relative position of anomalies (a) and the distribution of anomaly lengths (b) in the test set of different time series in SMD.

and usually not even 500 time steps. Most time series contain only few anomalies, making any definitive statement on their distribution difficult. One time series even contains just one anomaly. Time series, for which we can identify positional bias include: machine-1-1, machine-2-1, machine-2-2, machine-2-9, and machine-3-8.

Most time series suffer from consistently constant features, see Figure 22. Several of the constant features are constant for all time series. Since we cannot say for certain what those features represent due to the lack of documentation, we are reluctant to outright remove those features. We do not expect the performance to suffer much from their inclusion as they make up only very small percentage of features.

In several time series we have found possible delayed effects of anomalies, see Figure 23. In other time series we strongly suspect anomalies had long term effects on the system, see Figure 24. For most instances we can observe the effects across multiple features. That and

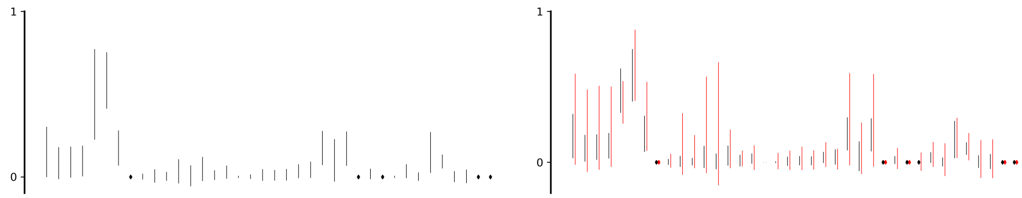

(a) Train set feature distribution (b) Test set feature distribution

Figure 22: Example of the feature distribution of a time series in SMD.

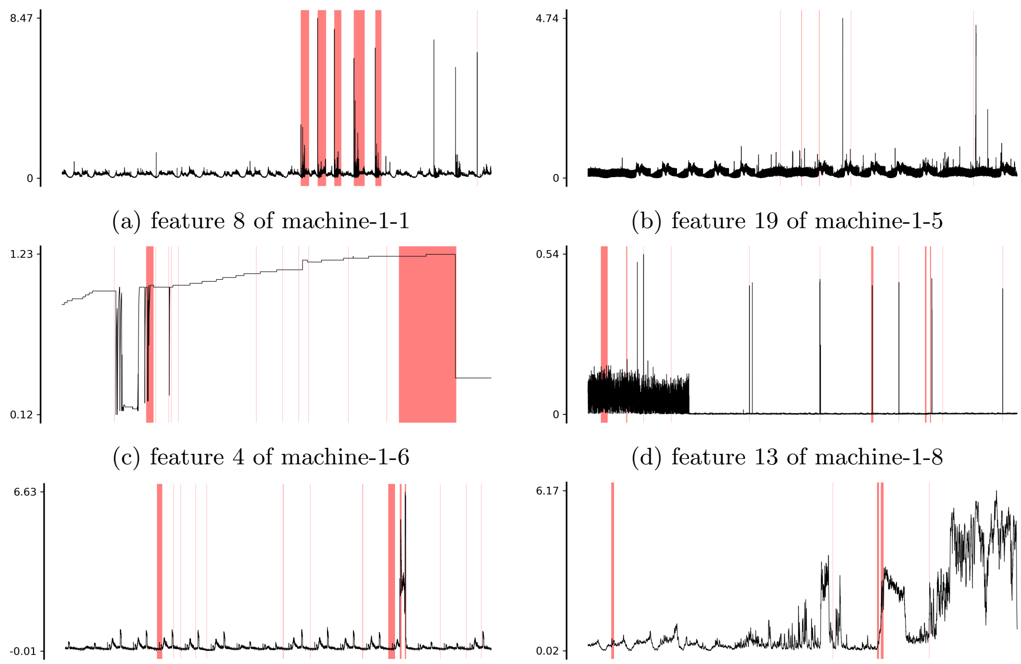

(a) feature 8 of machine-1-1 (b) feature 19 of machine-1-5

(c) feature 4 of machine-1-6 (d) feature 13 of machine-1-8

(e) feature 15 of machine-2-5 (f) feature 3 of machine-3-5

Figure 23: Instances where we suspect anomalies had delayed effects.

the unusual ranges seem to affirm our assessment.

For one time series in particular, we could observe a feature dropping to zero and staying constant directly after an anomaly occurs, see Figure 25. However, we can also observe a constant period at the start of the training set. This effect might be caused by a startup period in the training set and a crash in the test set. Without full knowledge of the underlying process we can not give a definitive judgment on this case. However, this illustrates, that this dataset needs to undergo careful scrutiny by experts familiar with the underlying process. Until then we exclude machine-1-1, machine-1-3, machine-1-4, machine-1-5, machine-1-6, machine-1-8, machine-2-5, machine-2-8, machine-3-4, machine-3-5, machine-3-7, machine-3-10, and machine-3-11 from our final report. However, we still evaluate and report on all datasets from SMD. We will provide the missing results in Appendix E.

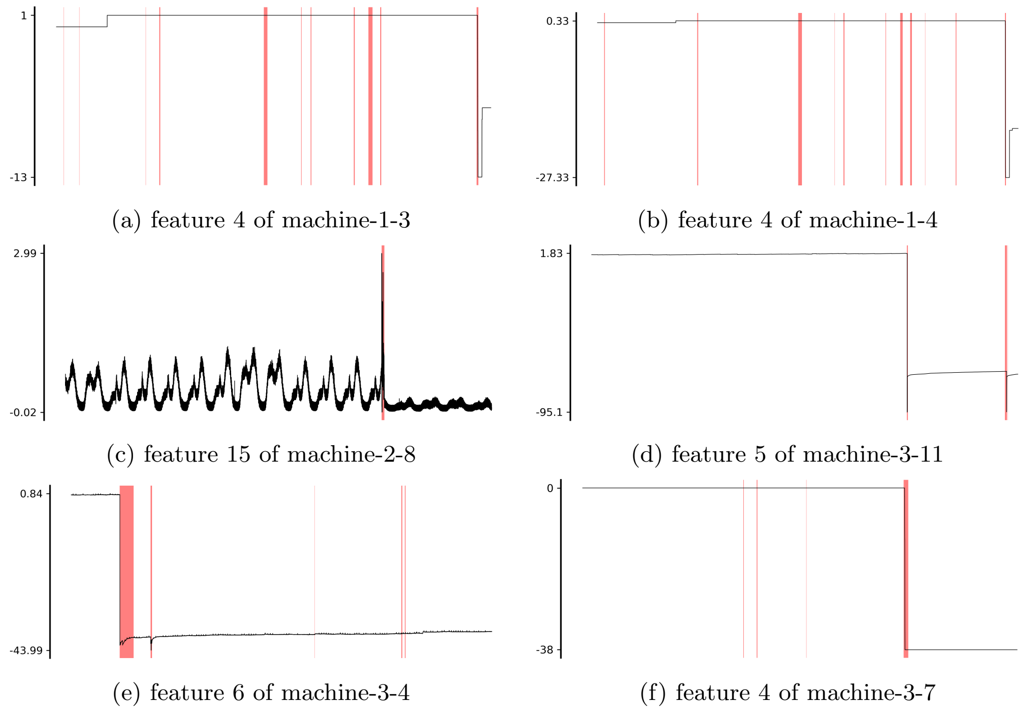

(a) feature 4 of machine-1-3

(b) feature 4 of machine-1-4

(c) feature 15 of machine-2-8

(d) feature 5 of machine-3-11

(e) feature 6 of machine-3-4

(f) feature 4 of machine-3-7

Figure 24: Instances where we suspect anomalies had long-term effects.

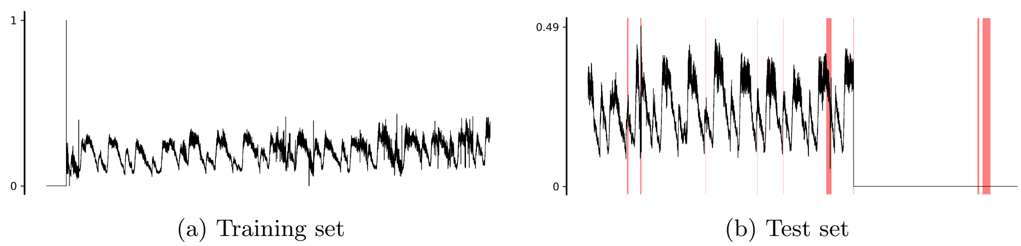

(a) Training set

(b) Test set

Figure 25: Feature 34 of machine-3-10.

B.6 Exathlon

The Exathlon dataset (Jacob et al., 2020) was created from ten applications running on a Spark cluster with four nodes. The authors collected 2,283 metrics from the monitoring system and the underlying operating system. They remark, that the collected metrics could very well be correlated and suggest a curated subset of 19 features to use instead. Furthermore, in their implementation, they remove all time series from two applications (ids 7 and 8). One application contains no anomalies in the test set and the other has no training set. Thus, we only consider applications 1-6 and 9-10. The final dataset thus consists of eight datasets, each consisting of the execution traces of a single application. For the test set, they insert six types of anomalies in the cluster. One anomaly in particular, uses up memory until the application crashes due to memory constraints, which means at least seven timer series suffer from positional bias, which is generally weakened by the other time series of each application. A detailed description of all applications and anomalies can be found on the GitHub page of the original implementation[8].

Overall we find a slight positional bias in several datasets, mostly attributed to the one anomaly discussed prior. We found no consistently constant features throughout the entire dataset. Most time series in the dataset contain unusual spikes, which the authors attribute

[8] `https://github.com/exathlonbenchmark/exathlon/wiki/Dataset`

to background activities on the cluster. Since such background activity is considered normal we ignore such cases in general. However, we would like to draw attention to one particular instance, where the spike reaches a new high directly after an anomaly occurs, see Figure 26. Since the effect of this spike is reflected in multiple features and we found no other such

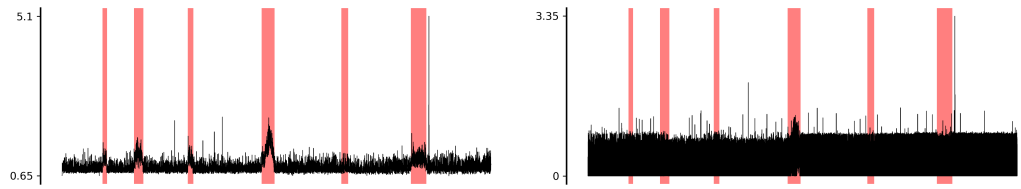

(a) driver_StreamingMetrics_streaming_lastCompletedBatch_processingDelay_value (b) 1_diff_avg_executor_runTime_count

Figure 26: Two features from a time series in the test set of application 1 in Exathlon. The anomalies injected in this time series are of the type cpu_contention anomaly.

example, we believe this instance warrants a closer inspection by experts in the future.

In total, we omit only one additional application. In the test set of application 10, we can observe a strong distributional shift in one feature, see Figure 27. Since this change persists

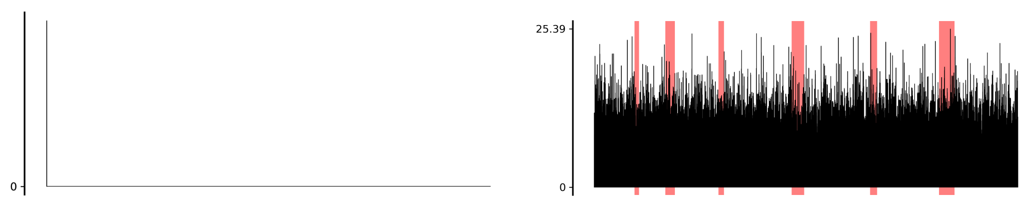

(a) Feature in train set (b) Feature in test set

Figure 27: Feature 1_diff_avg_executor_shuffleRecordsRead_count of a time series in the test set of application 10.

throughout the entire test time series independent of any anomalies present, we suspect this might be unintentional. We still report our results on this application in Appendix E, but exclude the application from our main evaluation. Lastly, we also omit application 3 from our main evaluation. The time series in the test set of this application are comparatively short, leaving only about 500 to 1,000 time steps for evaluation folds. Together with sparse anomalies, leaves several folds with no anomalies at all, complicating the evaluation.

C Methods

Most approaches, in particular recent ones, rely on a combination of multiple architectural elements. Thus we focus on the method for computing the final anomaly scores. In our setting, we expect each method to compute an anomaly score for each time step based only on the knowledge from prior time steps. Some methods are built to compute anomaly scores for entire time-series or windows. For most we can adapt the method to produce local scores based on the context of a window. We discuss global methods separately at the end of this section. In the following, we will discuss each class of methods in its own section.

C.1 Reconstruction-based methods

Based on the idea of the classical autoencoder (AE), some methods use an encoder network followed by a decoder network to map the input data into a smaller latent space and back into the input space. The idea is based on the intuition, that the information in the latent space should be enough to adequately reconstruct the input data, and, because the latent space is smaller than the input space, the networks can thus not simply learn an identity function. Since the method is generally only trained on normal data, we expect the reconstruction to fail for anomalous inputs. Thus, such methods rely on the reconstruction error to compute the anomaly score. Most of the time, the mean squared error (MSE) is used to train such methods and is later used for the anomaly score as well. Since squaring is strictly monotone for non-negative values, the resulting order is equivalent to the absolute error, which is sometimes used in its stead.

LSTM-AE Malhotra et al. (2016) propose to use an LSTM network as the encoder and as the decoder. The decoder LSTM takes the final hidden state of the encoder LSTM as the initial hidden state and reconstructs the input in reverse order. During training, it uses the true input data as inputs, but during testing, it uses its own predictions.

LSTM-Max-AE Mirza & Cosan (2018) propose to use use the mean or maximum of the hidden states of the encoder instead. Additionally, they use the latent representation as input for all time steps during reconstruction. Contrary to Malhotra et al. (2016) they reconstruct the inputs in the same order.

MSCRED Instead of raw inputs, Zhang et al. (2019) capture the correlation of time-series segments in signature matrices before applying a fully 2D-convolutional network and feeding its output into a 2D-convolutional LSTM encoder and decoder.

USAD Audibert et al. (2020) use two autoencoders with a shared encoder. Training consists of two phases: First, both train to minimize the reconstruction error. Afterward, training shifts to an adversarial setting. Here, the second autoencoder aims to distinguish real samples from those generated by the first autoencoder, whereas the first autoencoder tries to fool the adversary. During inference, a combination of reconstruction and adversarial loss yields the anomaly score for each point.

TCN-S2S-AE Thill et al. (2020) propose a fully convolutional AE architecture with a temporal convolutional network (TCN) in the encoder and a transposed TCN in the decoder. Instead of the usual MSE loss, they use the LogCosh loss as their training objective. A Gaussian is fitted on the errors over the test set during testing. However, this avoids using the method in an online setting. Therefore, we fit the Gaussian to a held-out validation set to be comparable to other methods.

IDEAL Homayouni et al. (2020) propose another LSTM-based AE that determines its ideal window size based on the input time serie's autocorrelation. However, it seems to us that eq.(2) in the paper has some mistakes, as there is a sum over index i and i is never used and the authors attempt to compute a confidence interval using the cumulative distribution function of a standard normal distribution instead of its inverse. Furthermore, the authors do not specify any details regarding the dimensionality of the latent space and how the decoder uses the latent vector to produce the reconstructed sequence. Thus, we cannot implement IDEAL for our library.

GenAD Hua et al. (2022) split an input TS into 5 folds of equal size. During training, they mask a random fraction of input features in the last fold by replacing them with the values of another randomly chosen feature. After that, they apply several multi-head self attention layers to the masked input sequence. Each layer computes attention along the time and feature dimensions separately. Their outputs are interpolated with a learnable weight to produce the final reconstructed sequence. During training, GENAD computes the LogCosh reconstruction loss over the previously masked features. The paper does not clearly describe the detection procedure, hence, the following is what we implemented in the absence of specific details: We mask each feature in the input TS once and let the GENAD model compute its reconstruction. If the reconstruction error, measured by the LogCosh metric, is larger than some threshold, we consider that feature anomalous. Finally, if more than a predetermined fraction of the input features at a certain point in time is anomalous, we consider the entire TS to be anomalous at that time point.

STGAT-MAD [9] Zhan et al. (2022) process an input TS by applying several 1D-convolution layers with different kernel sizes before passing each of the resulting sequences through several graph attention and graph convolution layers in parallel. Then they concatenate the output of those layers and feed them to a bi-LSTM decoder, which attempts to reconstruct the original input TS. STGAT-MAD uses the squared error as both its training loss and anomaly score.

C.2 Prediction-based methods

Prediction-based methods—sometimes also called forecasting methods—attempt to predict the next $k \geq 1$ time steps, called prediction horizon, when given an input time series. After training on normal data, they should be capable of accurately predicting the next time steps as long as the input time series and the points that are to be predicted are not anomalous. However, if any point in the prediction horizon is anomalous, the model will usually produce a higher prediction error for those points. Methods in this category use this prediction error as the basis for their anomaly score. Most methods measure the prediction error in therms of the MSE or mean absolute error (MAE).

LSTM-P Malhotra et al. (2015) use a multilayer LSTM to extract features and an FC NN to generate l-steps ahead predictions. An MSE loss is used during training, and at inference, a multivariate Gaussian is fitted to the errors of the held-out validation set. Given the learned distribution, the negative log-likelihood corresponds to the anomaly scores.

LSTM-S2S-P Similar to LSTM-P, Filonov et al. (2016) use a multilayer LSTM. However, they use the hidden features at each time step to predict the forecast, making their model a sequence-to-sequence predictor. An exponentially weighted moving average of the reconstruction errors yields the anomaly scores.

DeepANT/TCN-P Munir et al. (2018) use a TCN with max pooling and an MLP after that to predict the next k points from the input window x. They train the model with the MAE. However, the anomaly score is simply the MSE between a point and its prediction. If the prediction horizon $k > 1$ and there are multiple predictions for a single time step, we take their average and compute the MSE for that.

TCN-S2S-P He & Zhao (2019) pass the input window through a dilated causal TCN and concatenate the outputs of the last three layers along the feature dimension to pass this to a final convolution layer with kernel size one and D filters. The output of their method is a window of size $w \times D$ shifted by one time step compared to the input window. TCN-S2S-P uses the MSE loss during training and fits a Gaussian distribution to the prediction errors,

[9] `https://github.com/zhanjun717/STGAT`

just like LSTM-P. Note that during detection, we can only use the last point in the predicted window due to the requirement that the detector must work in an online setting.

GDN [10] Deng & Hooi (2021) construct a graph with features as its nodes and edges representing relations between features. They train an embedding vector for each feature and add directed edges from each feature to the top $m \in \mathbb{N}$ features based on cosine similarity between the feature embeddings. Thus the graph is dynamically recreated for each input batch. After that, they apply a graph attention mechanism (Veličković et al., 2018) to this dynamic graph and pass the outputs to an MLP that returns the prediction for the next time step. The authors use the MSE as their training loss and the MAE, which they normalise using each feature's median and interquartile range, as their anomaly score. They compute the two statistics over the test set, making GDN an offline method. However, computing the statistics over held-out normal data performed poorly due to constant features in the datasets. Hence, we decided to use the unscaled MSE as the anomaly score instead.

C.3 Generative methods

Generative methods model the data-generating distribution directly by training a generative model on some latent space with a predefined prior that produces samples close to the real data. Those models usually offer some way of computing the marginal likelihood of a data point under the model they learned, which can be used to derive anomaly scores.

C.3.1 VAE-based methods

LSTM-VAE Sölch et al. (2016) choose both the likelihood $p(x \mid z)$ and the posterior approximation $q(z \mid x)$ to be Gaussian and instantiate all NNs as single-layer LSTMs. Their encoder returns a mean and covariance component for each time step. Furthermore, they use $p(z) = \mathcal{N}(\mu, I)$ as a prior, where $\mu = (\mu_1, \ldots, \mu_T)$ is produced by another LSTM. The anomaly score is the negative ELBO.

Donut [11] Xu et al. (2018) chose to use MLPs for both encoder and decoder. Furthermore, they mask some time steps in the input by setting them to zero. During training, Donut maximizes a modified version of the ELBO that accounts for the input masking. Their anomaly score is the so-called "reconstruction probability" $\mathbb{E}_{z \sim q(z|x)}[-\log p(x \mid z)]$, although they combine it with elaborate mechanisms to reconstruct missing data. However, those are not relevant to this work since we do not have to deal with missing data. Note that the original formulation only supports univariate TS. We extend it to the multivariate case by simply applying the MLPs to the flattened multivariate input window, and we do not mask entire time steps but random features in random time steps instead.

LSTM-DVAE Park et al. (2018) apply zero-mean Gaussian noise to any input before feeding it to the encoder, and their prior mean for each time step is computed as

$$\mu_t = \left(1 - \frac{t}{T}\right) v_1 + \frac{t}{T} v_T,$$

where $v_1, v_T \in \mathbb{R}^{D'}$ are learnable parameters of the model. Furthermore, they use the reconstruction probability as their anomaly score. Apart from that, the method is exactly the same as the LSTM-VAE.

GMM-GRU-VAE Guo et al. (2018) use GRUs for both their encoder and decoder. Additionally, they chose a Gaussian mixture distribution with K components as their variational posterior approximation. Their prior is also a Gaussian mixture with learnable parameters μ_k, Σ_k for each of the K components. GMM-GRU-VAE uses the reconstruction probability as its anomaly score.

[10] `https://github.com/d-ailin/GDN`
[11] `https://github.com/NetManAIOps/donut`

BI-LSTM-VAE Pereira & Silveira (2018) propose to use a bi-directional LSTM for both encoder and decoder. They compute mean and variance for the latent Gaussian distribution from the last hidden state of the encoder. Additionally, the authors apply self-attention to the sequence of encoder hidden states and use the results to instantiate another Gaussian distribution at each time step. The samples from those distribution are combined with the sample from the original latent distribution at each time step to form the input for the decoder. However, the paper does not mention how exactly this sample is combined with the samples from the attention results at each time step. We contacted the authors on this matter but did not receive any response. Thus, we decided not to implement BI-LSTM-VAE as part of our library.

OmniAnomaly [12] Su et al. (2019) use a GRU-based encoder and decoder. They also apply a planar normalising flow (Rezende & Mohamed, 2015) to the latent variable z after they sample it from a multivariate normal distribution with parameters defined by the encoder. Furthermore, they choose a linear Gaussian state space model, i.e., a Kalman filter, for the prior $p(z)$. OmniAnomaly also uses the reconstruction probability as its anomaly score.

SIS-VAE Li et al. (2021a) propose another GRU-based VAE. They encourage the VAE to reconstruct smooth TS by adding a KL-divergence term between adjacent time steps term to the ELBO. Intuitively, this term encourages that the distributions for two neighbouring points in the predicted TS are similar to each other. Like most other VAE-based methods, SIS-VAE uses the reconstruction probability as its anomaly score.

C.3.2 GAN-based methods

BeatGAN [13] Zhou et al. (2019) use a TCN-based AE as the generator and a TCN-based discriminator. Technically speaking, their method is not really generative since they simply pass the input TS x through a deterministic AE and treat the reconstructed sample $\hat{x}$ as the "generated" input for a GAN discriminator. Furthermore, they only use the reconstruction error (MSE) of the AE as their anomaly score, completely discarding the discriminator after training. Nevertheless, we decided to put BeatGAN in the GAN category because it shares some architectural elements with the other GAN-based approaches. However, it would also be justified to think of BeatGAN as a reconstruction-based method with adversarial regularisation, similar to USAD. The TCN AE trains to minimise the MSE between input x and reconstruction $\hat{x}$ as well as the MSE between their feature maps in the discriminator's second-to-last layer. The discriminator, on the other hand, is trained on the standard GAN loss. Note that the authors augment the input dataset during training by applying dynamic time warping (Vintsyuk, 1968) to each input window and concatenating the resulting distorted window to the original dataset.

MAD-GAN [14] Li et al. (2019) use LSTMs as generator and discriminator in their GAN-based approach. Besides the usual discriminator score, they also use a "reconstruction" score. They start with a random latent variable $z \sim \mathcal{N}(0, I)$ and pass it through the generator to obtain $\hat{x}$. Now they use a Gaussian/RBF kernel to compute the similarity between the current input x and the generated sample $\hat{x}$ and use $1 - \text{sim}(x, \hat{x})$ as the reconstruction error. They minimise this error using gradient-based methods on z until it falls below a certain threshold. Then, they compute the MAE between original and reconstructed input and use it as the anomaly score together with the discriminator's output.

Conv-GAN Jiang et al. (2019) extract a fixed set of 16 features from an input time series and pass this vector trough a fully convolutional AE. Like BeatGAN, they consider the reconstructed vector as their "generated" sample. Conv-GANS's discriminator is also a CNN. Furthermore, they add an additional encoder to the generator that takes the reconstructed input and transforms it to the latent space again, trying to match the latent vector of the

[12] `https://github.com/NetManAIOps/OmniAnomaly`

[13] `https://github.com/hi-bingo/BeatGAN`

[14] `https://github.com/LiDan456/MAD-GANs`

original AE. However, from table 3 in the paper it seems that the authors input the 16 extracted features as a 4×4 matrix into the model, but they do not specify which extracted feature goes where in the matrix. Furthermore, they also write that they do not use any feature extraction on some datasets but do not specify how the model works in that case. Thus, we decided not to implement Conv-GAN.

LSTM-VAE-GAN Niu et al. (2020) use the decoder of an LSTM-based VAE as the generator of a GAN with an LSTM discriminator. Instead of computing the likelihood of the VAE's output on the input x directly, they pass both original and reconstructed sequence through all but the last layer of the discriminator. The discriminator should not just be capable of detecting a transformed sample generated from a standard normal distribution but also transformed samples from the posterior approximation. Therefore, its loss has an additional term to detect samples from the posterior approximation.LSTM-VAE-GAN's anomaly score is a convex combination of the MAE between x and its reconstruction, and the negative discriminator score.

TadGAN [15] Geiger et al. (2020) propose to use bidirectional LSTMs as decoder and encoder of an AE. Additionally, they consider both the decoder and the encoder as generators of two separate Wasserstein GANs (Arjovsky et al., 2017). One GAN uses the decoder as its generator, which maps random samples $z \in \mathcal{N}(0, I)$ to the input data space, and its TCN-based discriminator then attempts to distinguish a real input x from the generated sample $\hat{x}$. However, the generator of the second GAN is the encoder, which maps a data point x to the latent space. The TCN discriminator of that second GAN must now distinguish if its input is a random sample from a standard normal distribution or an encoded data point. Note that the loss function also contains the reconstruction error of the AE measured by the MSE. The authors compute both the MSE and the discriminator score during detection and normalize both using their means and standard deviations in the test set. After taking the absolute value of both, they return a convex combination of the two scores as their final anomaly score. Like in the case of TCN-AE, we compute the statistics of both scores during training on a held-out part of the training set instead, turning TADGAN into an online method.

C.4 Hybrid methods

Some methods cannot be clearly assigned to one of the classes mentioned above, since they use principles of more than one class. For example, models could compute both reconstruction and prediction error for an input time series before combining them into a single anomaly score. We decided to place such methods in their own "hybrid" category.

LSTM-AE OC-SVM Said Elsayed et al. (2020) train an AE with multi-layer LSTMs as encoder and decoder. However, instead of deriving their anomaly score from the reconstruction error of the AE, the authors train an OC-SVM (Schölkopf et al., 2001) on the latent vectors produced by applying the encoder to the held-out clean validation set instead. This OC-SVM then yields the anomaly scores during detection. Note that we return the raw scores, i.e., a point's signed distance from the OC-SVM's separating hyperplane, instead of predictions (0 or 1) to stay consistent with the other methods in this thesis and to avoid putting the OC-SVM at a disadvantage by using a fixed threshold. Unfortunately, the authors do not describe how they pass the latent vector to the decoder in detail, so we decided to use the same architecture as the LSTM-Max-AE. Although this method shares many similarities with some of the reconstruction-based methods (especially LSTM-AE and LSTM-Max-AE), we do not consider it a reconstruction-based method since its anomaly score is not derived from the AE's reconstruction error.

[15] `https://github.com/sintel-dev/Orion`

MTAD-GAT Zhao et al. (2020)[16] apply two graph attention modules (Veličković et al., 2018) on top of a TCN, one taking features as nodes and one taking time points in a window as nodes. Both feed their output concatenated to the original input into a GRU. Unlike GDN, they just use a fully connected graph as the input and do not build a dynamic graph. The final hidden state of the GRU serves as the input for an MLP to predict the next time point and as the latent variable for a VAE with an MLP decoder. They additively combine the MSE of the prediction with the VAE's ELBO loss to train the model. The anomaly score also combines the MSE of the prediction and the reconstruction probability of the VAE using a trade-off coefficient $\gamma \in [0, 1]$.

C.5 Other methods

We list methods that do not fall into any of the above categories here. This includes, for example, one-class approaches, which are more widely used for AD on other data types.

GRELEN Zhang et al. (2022b) use multi-head self attention along the feature dimension to encode an input TS. More specifically, they compute the attention weights but use a softmax normalisation along the attention head axis. Those weights are then used as probabilities for a Gumbel softmax distribution, which the authors sample from. They consider this sample as h adjacency matrices, where h is the number of attention heads. GRELEN uses those adjacency matrices as inputs to a DCGRU (Li et al., 2018b) layer that aims to predict the next time step for each point in the input TS. During training, GRELEN uses a VAE style loss, where the DCGRU output is the mean of a normal distribution with constant variance and the Gumbel softmax distribution is considered the latent distribution. During testing, GRELEN uses the KL divergence between the latent distribution and a predefined prior. However, the paper lacks many important details, e.g., the value of the constant variance, and we could not understand how a second anomaly score described in the paper works.

[16] The authors included a link to `https://github.com/Azure/Multivariate-AD` in their paper, claiming that this repository contains their code and data, but as of now (27.09.2022) it is just an empty repository.

D Details about our evaluation procedure

Each time-series AD dataset consists of an unlabelled training set $\mathcal{D}_{\text{ul}} := \{x^{(1)}, \dots, x^{(N)}\}$, where each $x^{(i)} \in \mathbb{R}^{T_i \times D}$ is one time series and a labelled test set $\mathcal{D}_{\text{l}} := \{(x^{(1)}, y^{(i)}), \dots, (x^{(N)}, y^{(N')}\}$, where $x^{(i)} \in \mathbb{R}^{T_i \times D}$ and $y^{(i)} \in \{0,1\}^{T'_i}$ are the ground truth anomaly labels. We split the unlabelled data into two distinct sets $\mathcal{D}_{\text{train}}$ and $\mathcal{D}_{\text{val1}}$ such that $\mathcal{D}_{\text{train}}$ contains 75% of the available time points and $\mathcal{D}_{\text{val1}}$ contains 25%. If $N > 1$, we can achieve this split (approximately) by assigning the entire time series to either set. However, several datasets (e.g., SWaT, WADI, SMD) contain only as a single time series in both their labeled and unlabelled data. Hence, we decided to split each time series along the time dimension and assigned the resulting sub-sequences to $\mathcal{D}_{\text{train}}$ and $\mathcal{D}_{\text{val1}}$, respectively. We train each method for up to 100 epochs on $\mathcal{D}_{\text{train}}$, using early stopping on the validation loss calculated over $\mathcal{D}_{\text{val1}}$ for all methods except USAD and the GAN-based approaches. Some methods also require $\mathcal{D}_{\text{val1}}$ for fitting parameters of their anomaly detection module, e.g., mean and covariance matrices over reconstruction errors to use in a Gaussian distribution. USAD, BeatGAN, MAD-GAN, and LSTM-VAE-GAN use neither early stopping nor do their detectors require any parameter fitting, so we train them on the entire unlabelled data.

Since we perform a grid search to tune each method's hyperparameters, we also need to split the labeled data into another validation set $\mathcal{D}_{\text{val2}}$ and a test set $\mathcal{D}_{\text{test}}$. Using a simple split here might introduce an unwanted bias into our evaluation for the case where only one time series of labeled data is available. In this case, the anomalies in the validation set might be of a different type compared to the ones in the test set. Since the split is arbitrary, this might put some methods at an unfair disadvantage if we report only the scores on the test set. We cannot entirely eliminate this issue, but we attempt to mitigate it by performing a modified 5-fold cross validation. For that, we split the time series into five equally sized folds and use each fold as the validation set once. The remaining folds, excluding the ones directly next to the validation fold to reduce possible statistical interdependencies, form the test set. We choose the hyperparameters that perform best on the validation set in terms of the best F_1*-score and evaluate the corresponding model on the test set. The scores reported in our tables are averages over all five folds. To ensure a fair comparison between methods that incorporate their run time/computational complexity, we adapt the hyperparameter grid size of each method, s.t. it takes roughly 48h to evaluate them on a dataset collection like Exathlon or SMD. We provide the hyperparameter grid for each method as part of our source code repository[17].

All methods use sliding windows as their inputs, although window size and step size may differ between them as we consider them to be hyperparameters. Furthermore, we subsample the Exathlon dataset by partitioning each time series into windows of size five and computing the mean over each window.

We implemented all methods and datasets as part of our TimeSeAD library based on PyTorch (Paszke et al., 2019). To keep track of our training and evaluation experiments, we also developed a plugin for our library based on sacred (Greff et al., 2017). This plugin automatically saves all results, configuration, random seeds, and artifacts, e.g., model weights, that our experiments produce. Furthermore, we provide a list of all packages we use with their corresponding version numbers as part of our source code repository[17].

[17]We provide the code in the supplementary material, and later through a GitHub link.

E Detailed Benchmark Results

In the following, we present additional results from our benchmark experiments. Table Table 3 shows the ranked average scores for Exathlon and SMD. Here, we average the scores for both, Exathlon and SMD, only over the datasets, which we think fit the purpose of evaluating time series AD methods. Details about why and which specific datasets are excluded can be found in Appendix B. In order to fit on one paper, we use the following abbreviations: (1) F_1^{pw} $AUPRC^{pw}$ stand for the point-wise best F_1 score and area und the precision-recall curve (AUPRC), respectively, (2) for the appropriate F_1 and AUPRC introduce by (Tatbul et al., 2018), and, (3) for our modified metric.

Table 4, Table 5 and Table 6 display detailed results for Exathlon based on point-wise, (Tatbul et al., 2018) and our metric, respectively. Whereas, Table 7 to Table 12 show results on the SMD dataset. For a clear visual appearance, all scores are multiplied by 100. Note, that due to spacial constraints we have limited ourselves to only present the SMD datasets which we find to be best applicable for evaluation. See Appendix B for a detailed analysis on which and why we ignore specific datasets. Full results on all SMD servers will be made available with the publication of our library on GitHub.

Table 3: Ranked average scores of relevant datasets for Exathlon and SMD on six different evaluation metrics.

	Exathlon						**SMD**					
	F_1^{pw}	$AUPRC^{pw}$	F_1^{ts}	$AUPRC^{ts}$	F_1^{our}	$AUPRC^{our}$	F_1^{pw}	$AUPRC^{pw}$	F_1^{ts}	$AUPRC^{ts}$	F_1^{our}	$AUPRC^{our}$
LSTM-AE	21	20	14	20	22	21	**1**	**1**	5	**1**	**1**	**1**
LSTM-Max-AE	14	13	12	17	20	16	21	22	19	19	17	20
MSCRED	**1**	**3**	**3**	**1**	**1**	**3**	16	13	8	13	20	19
FC-AE	5	4	21	12	10	4	7	9	14	5	7	8
USAD	8	5	19	14	15	5	19	17	12	14	15	16
TCN-AE	4	17	**1**	**2**	**3**	17	18	24	**2**	24	21	24
GenAD	**3**	**1**	25	4	4	**1**	24	14	25	12	24	14
STGAT-MAD	6	6	10	6	14	9	5	4	7	4	5	4
LSTM-P	22	22	5	24	24	24	**2**	**2**	4	**2**	**2**	**2**
LSTM-S2S-P	18	21	**2**	**3**	11	22	13	15	**1**	10	18	21
DeepAnt	10	10	15	8	7	7	10	10	16	11	12	10
TCN-S2S-P	19	19	11	13	19	19	**3**	**3**	6	**3**	**3**	**3**
GDN	**2**	**2**	13	10	**2**	**2**	9	6	13	8	10	9
LSTM-VAE	11	11	20	16	6	11	11	11	18	15	9	11
Donut	15	16	4	9	16	15	6	5	11	6	6	6
LSTM-DVAE	16	15	22	23	17	18	12	19	22	22	13	15
GMM-GRU-VAE	7	12	16	21	5	10	4	8	10	7	4	5
OmniAnomaly	23	24	17	22	21	20	15	16	21	21	11	12
SIS-VAE	13	8	9	11	12	6	8	7	15	9	8	7
BeatGAN	20	14	24	19	8	8	17	18	17	17	16	17
MAD-GAN	12	9	18	18	18	14	23	23	**3**	18	23	23
LSTM-VAE-GAN	17	18	7	7	13	13	22	20	23	23	19	18
TadGAN	9	7	8	5	9	12	20	21	9	16	22	22
LSTM-AE OC-SVM	25	25	23	25	25	25	25	25	24	25	25	25
MTAD-GAT	24	23	6	15	23	23	14	12	20	20	14	13

Table 4: Cross-validation results on Exathlon evaluated with the point wise metric.

	Best F_1-score (point wise)									***AUPRC* (point wise)**								
	App ID									App ID								
	1	2	3	4	5	6	9	10	avg	1	2	3	4	5	6	9	10	avg
LSTM-AE	47.3	77.4	57.1	77.0	45.0	48.1	34.5	43.7	53.8 (20)	49.5	75.0	51.7	68.5	43.8	34.9	32.3	31.6	48.4 (19)
LSTM-Max-AE	64.0	63.1	55.4	76.1	45.1	50.8	47.2	45.2	55.9 (14)	69.9	60.8	51.6	73.8	42.8	36.4	38.0	38.2	51.4 (12)
MSCRED	65.0	72.3	79.1	90.5	50.4	63.1	48.9	54.3	65.4 (1)	57.0	66.3	75.9	89.1	48.0	40.9	44.2	46.9	58.5 (1)
FC-AE	64.4	62.4	55.2	85.5	48.5	54.5	42.3	46.9	57.5 (5)	69.7	61.6	51.3	83.9	45.9	38.9	39.7	40.4	53.9 (6)
USAD	61.8	62.2	49.5	87.7	52.1	53.3	38.5	48.3	56.7 (8)	67.2	61.5	46.8	84.1	48.4	40.4	36.4	40.5	53.2 (8)
TCN-AE	55.8	66.5	40.7	83.6	59.2	51.7	49.0	44.8	56.4 (12)	52.1	56.5	35.1	72.9	57.3	32.5	42.6	34.5	47.9 (20)
GenAD	68.5	57.4	42.4	91.7	50.9	68.5	34.2	38.2	56.5 (10)	70.8	59.4	52.1	84.7	51.8	67.0	37.9	32.4	57.0 (3)
STGAT-MAD	56.0	62.5	62.3	87.7	46.7	64.4	39.1	46.2	58.1 (3)	60.3	61.7	58.4	83.6	45.5	50.1	36.0	39.6	54.4 (4)
LSTM-P	47.9	71.2	46.5	75.2	47.4	38.4	41.0	43.4	51.4 (22)	48.7	66.2	50.5	62.6	46.3	25.3	38.2	29.2	45.9 (23)
LSTM-S2S-P	58.3	42.8	54.1	91.8	49.0	52.9	43.1	42.3	54.3 (18)	53.8	31.6	45.6	88.8	46.8	38.0	31.1	30.5	45.8 (24)
DeepAnt	57.7	60.4	45.9	89.2	50.3	55.1	41.4	46.2	55.8 (16)	62.8	54.7	39.3	84.1	49.5	39.0	38.1	38.2	50.7 (14)
TCN-S2S-P	53.1	67.5	53.3	86.0	44.8	47.7	38.1	39.6	53.8 (19)	56.2	62.5	52.6	77.7	44.0	32.1	35.2	28.2	48.6 (18)
GDN	74.8	64.3	68.2	83.3	47.7	55.4	48.5	48.8	61.4 (2)	79.7	62.6	65.5	80.5	47.4	38.5	43.1	42.0	57.4 (2)
LSTM-VAE	47.8	62.1	59.9	84.8	63.1	60.2	33.7	46.8	57.3 (6)	49.9	61.0	55.0	81.9	63.9	48.2	22.7	40.4	52.9 (10)
Donut	45.2	61.2	60.4	88.9	54.2	53.3	40.1	48.2	56.4 (11)	48.4	54.3	56.3	83.8	53.5	38.8	36.4	41.7	51.6 (11)
LSTM-DVAE	51.6	57.4	60.5	86.7	59.2	50.6	35.1	46.0	55.9 (13)	53.0	57.5	55.8	81.8	55.5	42.2	26.9	37.8	51.3 (13)
GMM-GRU-VAE	50.0	62.9	48.0	82.7	47.2	63.7	49.2	42.9	55.8 (15)	52.0	59.0	45.8	78.2	36.1	56.9	43.0	29.8	50.1 (15)
OmniAnomaly	45.5	58.5	62.0	41.0	61.6	62.3	40.1	44.3	51.9 (21)	42.9	59.0	59.7	31.1	60.3	51.2	35.7	40.0	47.5 (21)
SIS-VAE	51.9	61.7	63.9	88.3	51.1	58.8	36.8	43.8	57.0 (7)	57.2	61.2	59.0	84.9	48.3	44.4	33.8	38.6	53.5 (7)
BeatGAN	58.8	61.3	37.0	82.7	44.3	50.9	35.4	40.0	51.3 (23)	58.9	61.7	37.6	81.7	42.8	41.4	33.2	33.9	48.9 (17)
MAD-GAN	61.3	61.7	60.1	85.9	48.8	54.9	37.8	42.6	56.6 (9)	66.5	63.3	56.8	79.2	45.5	38.6	36.4	38.3	53.1 (9)
LSTM-VAE-GAN	58.6	56.1	57.2	89.3	35.1	54.6	45.2	45.4	55.2 (17)	57.8	51.4	52.4	87.5	30.4	41.0	40.8	33.6	49.4 (16)
TadGAN	74.8	62.6	65.3	80.1	48.9	50.3	38.4	44.1	58.1 (4)	79.4	61.4	60.1	77.8	44.6	37.7	34.3	37.3	54.1 (5)
LSTM-AE OC-SVM	51.3	67.2	36.3	73.8	41.4	38.7	35.0	40.8	48.0 (25)	52.7	64.4	29.7	63.0	35.4	30.6	32.0	35.1	42.8 (25)
MTAD-GAT	50.3	60.2	49.5	51.3	51.2	57.6	37.7	46.4	50.5 (24)	55.0	61.0	45.3	39.3	47.3	47.4	32.3	40.4	46.0 (22)

Table 5: Cross-validation results on Exathlon evaluated with the metric from Tatbul et al. (2018).

	Best F_1-score (Tatbull et al.)									***AUPRC*** **(Tatbull et al.)**								
	App ID									App ID								
	1	2	3	4	5	6	9	10	avg	1	2	3	4	5	6	9	10	avg
LSTM-AE	60.5	47.2	28.4	27.6	27.2	44.1	40.0	57.4	41.5 (20)	43.9	51.7	28.0	51.1	30.8	42.4	22.9	22.9	36.7 (22)
LSTM-Max-AE	61.6	47.6	45.0	35.3	17.3	25.5	61.7	66.0	45.0 (11)	49.0	41.8	39.2	73.0	31.5	33.6	27.7	24.6	40.0 (14)
MSCRED	68.6	69.4	76.4	72.1	48.7	64.9	77.0	56.1	66.7 (2)	67.2	60.7	60.9	86.7	49.1	58.1	52.0	39.0	59.2 (1)
FC-AE	62.3	37.9	44.8	33.8	20.9	32.5	45.1	61.0	42.3 (14)	50.4	38.8	30.6	71.9	34.3	44.6	27.1	24.9	40.3 (13)
USAD	51.0	38.9	54.7	38.2	26.5	38.3	45.3	47.8	42.6 (13)	49.7	39.8	39.7	72.1	37.5	42.4	23.4	25.7	41.3 (12)
TCN-AE	65.3	69.5	64.4	79.3	77.3	66.9	75.2	72.3	71.3 (1)	56.3	50.7	34.1	76.0	58.9	47.5	48.8	40.2	51.6 (2)
GenAD	38.1	34.8	37.5	54.3	19.3	34.0	16.4	34.3	33.6 (25)	53.4	47.1	42.6	81.9	38.4	75.2	28.8	25.1	49.1 (4)
STGAT-MAD	60.9	47.7	41.9	33.4	25.2	41.2	49.4	69.9	46.2 (7)	46.7	43.8	36.4	72.4	35.7	59.6	24.4	26.1	43.1 (7)
LSTM-P	57.7	49.7	39.1	26.4	26.7	45.1	79.0	68.5	49.1 (5)	43.0	48.9	17.0	48.1	34.5	27.9	32.7	27.7	35.0 (24)
LSTM-S2S-P	60.5	75.0	60.9	82.2	75.4	58.6	55.5	55.7	65.5 (3)	54.6	43.7	35.2	89.8	60.4	44.8	39.0	35.8	50.4 (3)
DeepAnt	60.5	44.5	46.2	38.2	32.9	38.5	31.2	46.4	42.3 (15)	49.2	41.7	29.3	72.6	41.3	49.9	24.8	24.9	41.7 (11)
TCN-S2S-P	54.8	52.8	36.3	27.5	32.4	45.1	42.7	61.1	44.1 (12)	45.9	44.8	25.3	64.8	36.2	45.7	27.8	20.9	38.9 (17)
GDN	61.1	41.8	35.9	32.9	24.1	38.2	48.6	50.9	41.7 (18)	57.3	38.5	39.9	69.0	36.2	44.2	31.7	24.9	42.7 (8)
LSTM-VAE	51.1	42.1	39.9	23.8	31.8	38.8	48.5	58.2	41.8 (17)	39.8	42.6	30.0	66.6	42.5	50.1	16.6	22.4	38.8 (18)
Donut	58.4	59.1	42.8	32.6	31.1	48.6	78.9	65.4	52.1 (4)	45.0	45.2	33.5	67.4	36.3	50.1	34.7	24.0	42.0 (9)
LSTM-DVAE	50.2	34.7	41.3	30.9	30.2	33.8	51.1	48.4	40.1 (22)	45.4	31.6	36.1	68.3	37.6	37.3	18.8	21.5	37.1 (21)
GMM-GRU-VAE	52.6	35.3	33.8	26.8	25.2	42.8	60.2	56.4	41.7 (19)	37.2	38.7	22.9	59.1	27.3	45.4	33.8	20.1	35.6 (23)
OmniAnomaly	58.6	35.3	43.3	21.6	33.8	36.1	57.3	42.1	41.0 (21)	52.0	40.0	39.9	27.7	43.1	50.2	26.9	20.2	37.5 (19)
SIS-VAE	56.1	33.9	43.5	36.0	33.9	39.8	63.5	68.5	46.9 (6)	43.5	39.5	38.3	73.3	39.0	50.4	28.6	23.3	42.0 (10)
BeatGAN	28.2	58.0	55.9	35.2	22.2	25.0	39.8	38.9	37.9 (24)	37.1	43.0	19.8	75.1	36.3	40.2	22.3	24.5	37.3 (20)
MAD-GAN	45.5	38.6	40.8	26.7	48.5	32.2	46.8	55.2	41.8 (16)	47.5	42.4	37.1	65.9	38.8	38.1	23.3	22.9	39.5 (16)
LSTM-VAE-GAN	58.4	56.0	46.4	45.1	30.2	40.1	43.5	49.7	46.2 (8)	50.1	45.7	35.9	77.9	30.6	42.4	34.6	28.9	43.3 (6)
TadGAN	56.7	48.4	49.9	43.1	47.4	32.1	38.2	49.4	45.7 (9)	60.9	47.1	38.8	75.8	45.7	39.8	29.4	26.5	45.5 (5)
LSTM-AE OC-SVM	50.5	30.4	36.9	49.0	30.1	37.3	32.6	46.4	39.1 (23)	39.8	38.0	30.5	55.6	34.0	30.2	22.0	19.7	33.7 (25)
MTAD-GAT	62.4	43.3	38.2	35.2	40.4	39.5	55.8	47.2	45.2 (10)	45.7	44.9	29.7	60.8	36.1	46.0	27.5	25.6	39.5 (15)

Table 6: Cross-validation results on Exathlon evaluated with our metric.

	Best F_1-score (ours) App ID 1	2	3	4	5	6	9	10	avg	***AUPRC* (ours)** App ID 1	2	3	4	5	6	9	10	avg
LSTM-AE	53.7	64.7	60.6	74.8	43.7	48.7	31.7	44.2	52.8 (23)	56.3	63.1	42.9	66.6	42.4	36.0	29.1	35.7	46.5 (21)
LSTM-Max-AE	67.3	50.8	59.1	73.2	44.0	51.7	41.5	37.4	53.1 (21)	72.2	49.3	53.6	72.7	44.4	40.4	33.9	31.6	49.7 (16)
MSCRED	64.2	64.7	84.0	90.9	49.0	63.5	50.1	54.8	65.1 (1)	56.4	62.4	29.8	89.6	47.7	41.6	44.4	48.3	52.5 (7)
FC-AE	68.1	52.1	71.3	84.0	47.4	55.1	38.9	42.6	57.4 (5)	72.8	52.7	69.9	85.4	47.8	42.7	37.8	36.7	55.8 (3)
USAD	65.5	52.6	54.6	85.6	51.3	53.4	34.4	43.8	55.1 (16)	70.4	53.4	56.5	84.3	50.0	43.6	32.9	36.8	53.5 (4)
TCN-AE	64.8	57.3	61.9	83.1	52.8	52.2	49.8	41.5	57.9 (3)	59.6	51.2	36.9	73.0	51.8	32.6	41.2	29.3	47.0 (19)
GenAD	70.6	47.7	42.4	89.7	52.3	68.0	25.2	33.1	53.6 (19)	74.5	53.1	51.6	87.2	53.1	67.4	35.7	32.3	56.8 (2)
STGAT-MAD	59.5	52.6	69.3	86.2	43.9	66.3	34.7	40.8	56.7 (11)	64.2	53.3	55.7	84.7	43.3	51.4	33.3	35.5	52.7 (6)
LSTM-P	55.1	54.1	68.6	73.2	52.8	38.3	37.3	43.1	52.8 (22)	57.5	53.2	55.2	61.4	51.5	26.0	34.5	32.6	46.5 (22)
LSTM-S2S-P	61.8	52.2	60.5	91.2	41.4	55.2	43.5	38.1	55.5 (14)	55.1	34.9	53.1	87.0	39.5	37.0	32.0	30.3	46.1 (24)
DeepAnt	63.4	54.8	64.7	87.3	51.0	56.0	36.6	41.0	56.8 (10)	66.9	50.5	47.2	85.1	49.9	42.9	36.2	33.4	51.5 (10)
TCN-S2S-P	58.3	56.5	68.8	83.7	50.0	47.7	34.6	38.4	54.8 (17)	62.0	54.7	35.2	76.0	48.1	32.1	33.2	30.9	46.5 (20)
GDN	76.5	56.9	69.4	81.7	46.6	57.9	46.1	42.5	59.7 (2)	80.4	55.4	68.7	82.0	45.1	44.3	40.5	38.4	56.8 (1)
LSTM-VAE	54.7	53.0	68.6	83.2	65.5	59.1	34.6	40.3	57.4 (6)	57.9	53.5	40.4	81.8	65.3	47.2	22.8	37.6	50.8 (14)
Donut	54.2	50.9	71.0	86.8	57.0	51.9	39.3	44.5	56.9 (8)	56.5	46.7	51.8	82.4	57.3	37.5	33.6	41.9	51.0 (12)
LSTM-DVAE	56.2	50.0	67.9	81.3	63.8	47.8	34.4	42.4	55.5 (15)	55.6	48.4	53.8	77.2	61.1	39.5	26.4	38.2	50.0 (15)
GMM-GRU-VAE	54.7	54.7	67.3	79.4	53.5	61.9	47.9	40.5	57.5 (4)	58.2	52.8	53.9	76.6	42.1	56.2	42.8	34.1	52.1 (9)
OmniAnomaly	53.4	51.6	69.5	44.7	68.3	62.3	37.8	39.5	53.4 (20)	53.5	52.7	57.2	37.9	67.4	51.7	33.4	35.4	48.7 (18)
SIS-VAE	56.8	52.7	70.3	88.2	53.0	61.1	32.4	38.8	56.6 (12)	61.6	53.3	55.9	87.1	52.1	48.7	30.8	33.9	52.9 (5)
BeatGAN	65.9	64.7	68.9	82.3	44.0	54.3	36.5	38.4	56.9 (9)	67.1	55.4	31.0	81.0	49.1	44.4	33.5	32.7	49.3 (17)
MAD-GAN	64.4	52.7	67.9	84.0	43.3	56.5	32.1	36.2	54.6 (18)	68.3	54.4	54.7	79.3	42.4	43.2	32.4	33.1	51.0 (13)
LSTM-VAE-GAN	63.9	55.7	62.1	89.3	39.5	54.0	41.6	44.7	56.3 (13)	67.0	49.7	49.1	89.7	35.4	42.5	37.9	38.3	51.2 (11)
TadGAN	78.6	58.8	70.4	77.7	46.1	52.7	33.0	39.5	57.1 (7)	82.7	54.3	55.1	75.1	44.0	40.8	31.5	34.3	52.2 (8)
LSTM-AE OC-SVM	57.5	54.9	46.0	71.7	38.5	39.7	29.1	37.2	46.8 (25)	58.2	53.1	48.9	63.5	33.3	32.4	27.3	34.2	43.9 (25)
MTAD-GAT	54.6	54.0	67.7	53.0	55.5	56.4	40.0	36.6	52.2 (24)	59.5	53.4	52.0	42.4	50.0	46.6	33.3	34.3	46.4 (23)

Table 7: Cross-validation results on SMD evaluated with F1 point wise.

	Server ID															
	1	6	8	9	10	11	13	14	16	17	20	21	24	26	27	avg.
LSTM-AE	47.1	68.9	29.4	33.9	60.4	30.6	56.8	64.5	51.9	74.6	14.7	42.3	65.3	23.4	78.1	49.5 (1)
LSTM-Max-AE	52.7	32.2	23.0	33.9	33.0	29.7	58.1	44.4	35.8	56.2	14.0	11.8	52.4	25.4	61.3	37.6 (21)
MSCRED	53.9	49.5	43.7	28.0	40.2	22.1	48.8	37.6	48.2	60.8	12.3	24.4	47.5	20.5	57.7	39.7 (16)
FC-AE	49.0	56.4	30.7	34.2	48.7	27.7	56.9	58.4	44.8	64.8	14.4	32.7	57.0	23.5	79.4	45.2 (7)
USAD	37.7	48.6	20.9	33.8	35.7	38.0	56.9	58.6	34.6	56.8	13.5	27.9	46.6	17.9	58.4	39.1 (19)
TCN-AE	47.0	52.7	36.6	23.9	33.9	23.6	44.7	35.9	44.4	63.3	16.8	24.2	55.2	31.5	52.8	39.1 (18)
GenAD	44.6	21.0	12.7	26.6	22.4	15.7	52.5	46.7	31.2	55.2	10.5	7.1	48.4	21.1	59.6	31.7 (24)
STGAT-MAD	48.1	64.5	24.2	34.7	55.9	26.6	56.7	58.1	49.5	65.6	15.9	33.0	59.5	25.4	78.2	46.4 (5)
LSTM-P	54.7	73.8	36.5	32.7	58.2	31.8	56.6	63.0	49.5	69.5	14.4	37.1	59.2	23.9	78.7	49.3 (2)
LSTM-S2S-P	53.0	54.5	43.1	27.2	28.2	28.7	43.8	34.8	47.7	54.4	14.4	34.8	58.0	29.5	55.7	40.5 (13)
DeepAnt	50.6	60.4	26.8	35.0	42.2	28.9	56.2	59.6	45.7	61.4	14.3	30.0	60.6	24.8	61.0	43.8 (10)
TCN-S2S-P	41.9	73.2	34.6	34.1	52.5	31.9	54.0	55.1	51.5	78.3	16.2	36.3	60.7	26.0	80.9	48.5 (3)
GDN	58.9	58.6	32.0	34.2	53.9	26.3	56.4	56.6	43.9	63.3	13.4	30.0	59.9	20.2	68.2	45.0 (9)
LSTM-VAE	45.7	62.1	22.9	26.7	60.5	32.0	57.7	54.1	44.9	50.0	14.5	39.2	57.2	21.9	63.9	43.6 (11)
Donut	42.7	62.8	27.6	35.4	63.2	40.0	50.1	60.9	40.6	70.7	17.1	29.5	64.3	14.5	74.1	46.2 (6)
LSTM-DVAE	40.1	61.3	24.0	23.4	51.7	35.7	52.8	62.2	42.4	39.1	15.7	38.0	58.7	22.9	49.0	41.1 (12)
GMM-GRU-VAE	44.4	64.2	25.3	34.1	62.0	36.0	55.6	58.7	40.3	71.2	16.1	32.1	60.2	22.9	77.7	46.7 (4)
OmniAnomaly	38.9	63.1	23.6	33.3	32.7	31.2	60.6	50.8	50.1	42.1	13.7	24.1	54.1	13.8	73.4	40.4 (15)
SIS-VAE	53.9	63.0	27.5	34.6	47.4	27.4	56.9	59.8	43.5	64.0	15.0	28.8	55.4	23.7	75.8	45.1 (8)
BeatGAN	44.5	48.8	24.1	33.2	45.5	33.2	57.0	45.1	38.3	58.8	13.4	24.7	42.8	23.0	57.8	39.3 (17)
MAD-GAN	41.5	33.9	30.2	33.9	44.6	20.3	38.8	45.7	42.4	47.6	15.4	9.8	32.1	25.7	32.7	33.0 (23)
LSTM-VAE-GAN	47.8	45.0	21.2	36.7	51.8	25.3	58.0	35.9	28.4	51.6	14.0	19.6	31.3	27.7	60.6	37.0 (22)
TadGAN	49.7	28.2	14.1	33.9	51.1	31.1	58.3	45.8	35.3	54.9	14.9	21.9	54.3	27.0	48.9	38.0 (20)
LSTM-AE OC-SVM	16.9	25.2	13.7	19.2	18.3	31.5	22.0	35.2	19.7	50.5	14.6	10.7	40.3	27.6	56.7	26.8 (25)
MTAD-GAT	40.3	67.8	13.2	33.2	51.6	50.2	44.8	47.7	40.7	39.8	12.6	31.9	50.9	26.5	55.1	40.4 (14)

Table 8: Cross-validation results on SMD evaluated with AUPRC point wise.

	Server ID															
	1	6	8	9	10	11	13	14	16	17	20	21	24	26	27	avg.
LSTM-AE	32.9	68.9	23.6	23.4	59.3	26.8	48.7	62.8	51.9	73.7	8.3	32.2	62.4	23.8	76.8	45.0 (1)
LSTM-Max-AE	41.6	17.2	20.3	23.2	21.5	26.2	49.4	35.6	35.9	54.0	6.5	7.0	48.9	24.6	57.5	31.3 (22)
MSCRED	48.3	36.6	41.0	15.0	25.7	16.2	42.8	47.4	45.6	60.2	5.7	19.3	47.1	17.4	55.5	34.9 (13)
FC-AE	42.0	46.1	26.2	24.7	41.8	22.8	47.1	51.7	42.7	63.5	5.4	24.1	53.6	23.6	77.6	39.5 (9)
USAD	31.3	39.6	15.7	21.3	29.7	36.8	46.8	50.4	28.4	54.4	7.1	19.5	42.6	18.5	54.3	33.1 (17)
TCN-AE	27.4	36.8	24.1	13.3	14.4	17.4	22.2	21.8	41.1	57.9	8.8	13.3	36.1	27.6	33.9	26.4 (24)
GenAD	40.6	21.3	25.8	19.3	35.3	23.0	49.7	55.5	34.6	60.9	8.7	12.6	50.5	20.8	55.4	34.3 (14)
STGAT-MAD	38.2	56.8	22.0	25.2	50.9	23.2	48.9	55.1	49.4	65.0	8.2	24.5	59.9	25.6	73.8	41.8 (4)
LSTM-P	48.3	71.8	29.4	23.7	54.9	29.7	49.1	54.2	50.2	67.6	7.6	28.0	59.5	23.1	75.5	44.8 (2)
LSTM-S2S-P	50.2	37.0	39.0	16.3	20.1	19.2	39.8	28.4	46.2	50.4	7.1	27.8	49.2	26.2	52.2	34.0 (15)
DeepAnt	42.0	52.3	21.3	25.2	35.2	23.3	48.4	52.9	43.6	58.3	6.5	18.7	61.7	24.0	58.7	38.1 (10)
TCN-S2S-P	31.0	72.3	27.2	24.0	47.2	29.2	48.0	46.7	51.6	76.7	9.1	27.1	60.5	23.5	77.3	43.4 (3)
GDN	50.6	50.6	28.4	24.0	50.7	23.8	48.6	48.9	40.6	61.3	5.9	19.4	61.6	20.2	64.7	40.0 (6)
LSTM-VAE	27.1	51.1	17.4	19.3	48.3	31.4	50.3	43.5	41.8	47.6	7.2	24.8	53.0	17.1	60.7	36.0 (11)
Donut	27.1	52.1	19.7	26.8	59.1	33.1	41.2	53.8	40.4	70.6	10.7	21.1	66.0	12.0	71.5	40.3 (5)
LSTM-DVAE	22.8	51.1	16.6	14.7	34.3	34.9	45.7	45.4	39.5	32.9	6.5	24.1	53.2	19.1	43.0	32.2 (19)
GMM-GRU-VAE	31.8	53.8	19.2	26.4	44.9	35.7	47.2	51.2	35.9	68.3	6.8	17.3	61.3	22.3	74.8	39.8 (8)
OmniAnomaly	22.2	54.1	17.7	26.5	18.0	28.4	52.2	36.8	52.0	41.3	8.3	12.5	56.2	10.0	70.5	33.8 (16)
SIS-VAE	43.8	57.9	22.2	24.8	41.5	22.3	49.2	53.6	42.7	60.9	6.4	19.8	55.0	24.1	73.3	39.8 (7)
BeatGAN	35.8	34.8	21.3	21.4	39.5	29.0	47.0	37.8	33.2	55.5	6.2	16.4	39.1	23.6	52.2	32.8 (18)
MAD-GAN	30.8	26.6	20.5	20.8	39.9	16.0	27.1	32.9	43.2	48.2	6.5	4.4	26.9	22.9	31.2	26.5 (23)
LSTM-VAE-GAN	38.7	37.3	18.1	30.5	46.2	16.4	51.0	33.4	31.2	49.0	6.9	13.6	25.4	29.1	55.9	32.2 (20)
TadGAN	34.7	16.3	9.1	22.1	44.3	26.8	47.5	40.4	31.2	52.0	8.0	13.0	51.4	24.9	48.6	31.4 (21)
LSTM-AE OC-SVM	8.4	19.7	9.9	9.2	12.8	23.7	13.3	28.2	17.5	45.8	7.5	4.8	32.1	26.7	48.3	20.5 (25)
MTAD-GAT	28.1	63.4	9.2	22.5	49.7	49.3	40.2	38.5	35.8	33.7	6.4	24.6	49.0	22.6	51.0	34.9 (12)

Table 9: Cross-validation results on SMD evaluated with the F_1 metric introduced by (Tatbul et al., 2018).

	Server ID															
	1	6	8	9	10	11	13	14	16	17	20	21	24	26	27	avg.
LSTM-AE	17.8	47.5	28.8	69.6	54.3	39.8	52.0	43.2	60.1	50.7	23.8	42.8	48.3	61.5	51.1	46.1 (5)
LSTM-Max-AE	26.7	50.3	22.5	72.8	35.7	15.0	54.4	25.7	62.9	34.6	14.4	15.6	45.5	59.3	35.3	38.0 (19)
MSCRED	37.9	37.4	36.9	58.6	41.5	32.9	50.3	9.7	61.7	71.2	25.1	8.1	52.4	64.4	64.9	43.5 (8)
FC-AE	23.1	36.1	24.6	66.3	31.1	26.5	53.3	42.9	58.2	45.6	26.5	33.1	46.7	53.7	42.8	40.7 (14)
USAD	25.8	43.2	29.3	76.3	44.3	20.9	53.1	42.6	57.9	36.8	19.5	29.3	53.4	59.2	42.2	42.3 (12)
TCN-AE	46.5	48.3	47.7	60.2	41.3	46.8	44.3	18.1	67.5	63.1	39.6	29.7	53.0	68.2	57.1	48.8 (2)
GenAD	23.4	17.0	22.6	53.7	29.0	5.9	47.1	33.1	51.6	25.4	4.7	2.8	43.6	56.9	38.1	30.3 (25)
STGAT-MAD	19.8	44.4	27.7	67.9	47.4	41.8	52.6	40.0	58.1	47.9	27.0	32.4	48.7	59.5	50.7	44.4 (7)
LSTM-P	34.0	55.1	30.6	68.7	56.7	44.0	53.2	40.4	55.2	52.4	22.1	35.5	51.9	55.1	49.4	47.0 (4)
LSTM-S2S-P	58.1	50.2	46.0	64.0	42.5	40.0	50.9	29.0	66.4	67.7	45.7	28.2	62.4	59.3	60.2	51.4 (1)
DeepAnt	23.3	39.3	27.0	66.8	28.1	23.8	52.3	42.2	58.0	52.6	20.7	30.0	44.1	51.1	38.9	39.9 (16)
TCN-S2S-P	16.2	51.3	29.5	70.0	47.1	46.2	51.2	31.3	54.8	61.1	29.6	34.9	48.7	49.3	58.1	45.3 (6)
GDN	24.7	40.1	25.5	62.2	35.7	27.9	52.4	39.9	63.3	41.4	22.7	30.7	44.6	65.2	38.2	41.0 (13)
LSTM-VAE	18.6	33.6	34.5	60.5	37.8	39.6	48.7	37.5	54.5	32.7	23.4	35.6	38.1	45.2	39.0	38.6 (18)
Donut	18.4	33.7	25.7	62.4	44.0	37.0	43.0	42.0	47.3	60.3	27.1	35.7	53.1	46.7	61.0	42.5 (11)
LSTM-DVAE	17.2	34.6	28.0	58.8	26.4	39.3	45.2	36.7	45.4	34.2	21.7	33.2	40.4	49.0	29.6	36.0 (22)
GMM-GRU-VAE	21.0	35.5	26.9	69.9	34.8	47.6	49.1	41.2	46.9	64.2	25.0	29.5	44.6	51.6	52.1	42.7 (10)
OmniAnomaly	17.6	30.7	31.4	67.1	15.6	41.8	45.6	31.9	49.4	45.9	16.7	20.3	33.2	41.4	52.0	36.0 (21)
SIS-VAE	24.6	37.6	26.2	63.8	30.4	29.1	52.7	44.0	59.3	40.4	22.1	31.2	47.0	54.0	42.1	40.3 (15)
BeatGAN	26.9	39.9	33.8	78.6	33.4	16.9	52.6	32.9	64.6	34.6	23.1	26.3	43.1	49.0	29.4	39.0 (17)
MAD-GAN	28.5	47.3	45.9	74.4	44.9	66.1	50.4	37.3	62.9	60.5	33.4	25.0	52.8	60.7	39.9	48.7 (3)
LSTM-VAE-GAN	20.7	35.4	23.9	63.9	33.6	22.2	52.4	16.0	52.8	29.1	20.3	38.1	33.6	53.6	33.3	35.3 (23)
TadGAN	33.6	35.1	41.7	72.3	30.0	27.1	55.7	32.6	63.5	33.5	18.9	37.7	52.7	59.0	46.9	42.7 (9)
LSTM-AE OC-SVM	9.9	27.0	21.3	51.9	11.4	18.5	21.3	9.9	62.5	53.7	26.3	32.1	32.4	56.1	58.4	32.8 (24)
MTAD-GAT	19.2	44.8	26.1	56.9	40.6	42.5	21.1	48.8	64.4	17.0	17.1	38.3	27.1	45.9	35.1	36.3 (20)

Table 10: Cross-validation results on SMD evaluated with the $AUPRC$ metric introduced by (Tatbul et al., 2018).

	Server ID															
	1	6	8	9	10	11	13	14	16	17	20	21	24	26	27	avg.
LSTM-AE	18.5	53.3	15.8	33.1	50.5	29.9	44.1	38.1	40.3	70.9	17.0	32.2	57.6	25.4	74.9	40.1 (1)
LSTM-Max-AE	28.4	24.6	12.8	30.9	23.5	11.4	45.7	13.3	37.5	53.4	5.9	7.4	53.0	28.7	55.8	28.8 (19)
MSCRED	38.0	28.3	25.4	13.4	23.8	15.8	45.2	20.9	33.8	69.7	8.6	4.9	52.6	25.2	62.0	31.2 (13)
FC-AE	25.3	35.8	14.7	30.2	29.1	18.2	44.2	31.3	39.8	60.5	10.7	21.1	53.8	26.3	71.7	34.2 (5)
USAD	21.2	39.2	12.5	31.1	25.6	19.3	43.3	31.3	30.6	54.3	8.2	17.6	49.4	24.7	58.3	31.1 (14)
TCN-AE	28.4	31.4	19.5	10.1	17.5	16.0	23.0	7.9	33.1	57.0	13.0	9.7	35.2	28.4	40.6	24.7 (24)
GenAD	27.4	25.3	25.1	22.4	39.8	16.2	43.4	41.5	31.5	56.5	10.0	13.2	50.9	26.3	49.2	31.9 (12)
STGAT-MAD	22.4	44.2	15.7	31.4	40.2	24.2	45.1	33.0	41.0	63.4	15.8	22.2	57.6	29.4	73.1	37.2 (4)
LSTM-P	35.4	59.4	17.9	33.2	46.6	32.3	46.8	29.0	34.3	68.6	13.5	24.0	58.1	21.4	75.5	39.7 (2)
LSTM-S2S-P	44.4	38.8	28.1	19.8	31.1	13.6	42.3	12.4	35.5	59.2	15.0	14.5	58.9	25.6	54.4	32.9 (10)
DeepAnt	24.6	41.3	14.6	30.8	27.8	16.6	43.8	29.9	39.6	56.3	11.0	14.3	54.8	24.4	55.0	32.3 (11)
TCN-S2S-P	18.2	55.3	16.7	32.8	41.2	33.8	45.1	21.2	35.6	72.9	18.4	21.8	54.2	18.5	75.5	37.4 (3)
GDN	29.8	39.3	15.8	28.7	33.1	16.1	43.5	28.5	40.5	54.6	10.0	18.3	52.4	30.7	55.5	33.1 (8)
LSTM-VAE	14.3	30.0	12.0	26.5	32.8	32.7	44.1	21.9	30.2	49.0	13.4	24.5	46.3	14.1	60.2	30.1 (15)
Donut	13.3	31.7	11.5	28.1	40.2	31.7	37.0	30.8	27.5	66.3	18.3	24.1	59.6	11.5	69.4	33.4 (6)
LSTM-DVAE	11.4	33.3	10.9	22.7	22.5	37.2	40.3	22.5	23.1	39.1	13.8	19.8	45.3	16.6	43.2	26.8 (22)
GMM-GRU-VAE	14.6	34.2	13.1	31.9	28.5	42.5	41.9	28.8	23.7	70.4	14.8	13.7	50.9	15.1	75.4	33.3 (7)
OmniAnomaly	10.9	32.0	11.5	33.6	9.8	35.1	40.5	13.8	31.3	59.6	10.7	9.2	46.0	10.1	68.0	28.1 (21)
SIS-VAE	25.5	40.7	14.5	30.4	28.0	18.4	44.1	32.2	39.5	53.7	10.6	17.7	49.3	25.6	65.7	33.0 (9)
BeatGAN	24.7	34.7	14.3	28.8	30.1	13.7	45.1	16.0	35.5	53.5	10.0	13.4	44.7	22.7	51.6	29.2 (17)
MAD-GAN	29.1	33.1	18.9	31.1	28.7	11.8	43.2	22.0	32.5	53.9	13.0	9.5	42.4	24.2	41.0	29.0 (18)
LSTM-VAE-GAN	23.0	35.6	11.7	31.7	27.7	9.5	45.3	7.1	32.3	43.9	7.9	12.3	30.4	27.2	53.4	26.6 (23)
TadGAN	32.7	19.8	13.1	32.3	29.4	12.4	44.9	17.6	41.1	51.7	9.6	11.7	53.2	29.6	50.1	29.9 (16)
LSTM-AE OC-SVM	5.6	20.6	6.8	7.7	6.6	10.7	13.9	4.5	25.9	46.9	7.7	7.3	29.6	26.5	52.9	18.2 (25)
MTAD-GAT	16.4	43.8	7.8	21.5	33.3	46.5	32.3	27.9	29.4	30.5	10.0	27.5	38.3	15.3	47.3	28.5 (20)

Table 11: Cross-validation results on SMD evaluated with our adapted best F_1 score metric, using $TRec^*$ and $TPrec^*$.

	Server ID														
	1	6	8	9	10	11	13	14	16	17	20	21	24	26	27	avg.
LSTM-AE	53.1	70.2	42.4	65.1	68.6	39.8	55.0	62.3	79.7	80.7	25.0	48.7	64.0	62.4	84.6	60.1 (1)
LSTM-Max-AE	55.8	28.6	30.3	64.8	34.9	24.6	54.3	26.1	63.1	68.8	16.1	10.6	58.8	61.4	72.4	44.7 (17)
MSCRED	51.3	46.3	47.0	58.5	36.1	14.0	47.0	10.1	70.3	73.0	14.3	14.4	52.1	54.3	64.3	43.5 (20)
FC-AE	52.2	61.1	40.3	65.1	51.0	29.8	53.0	48.2	75.7	77.2	18.0	36.4	60.3	61.2	85.4	54.3 (7)
USAD	43.0	45.0	31.7	63.9	36.0	33.2	52.9	45.2	59.4	68.1	18.7	26.3	52.4	53.7	68.6	46.5 (15)
TCN-AE	43.7	49.4	42.1	56.1	34.4	17.1	44.3	17.2	67.1	63.5	23.1	19.1	51.4	66.7	56.1	43.4 (21)
GenAD	44.8	17.7	26.6	50.6	28.2	12.3	53.8	25.7	60.2	61.7	5.3	2.9	53.6	58.3	68.9	38.0 (24)
STGAT-MAD	48.3	66.5	36.4	66.0	62.6	34.1	52.5	52.5	77.9	77.0	24.0	34.7	60.6	65.0	83.8	56.1 (5)
LSTM-P	61.7	73.4	46.7	64.2	61.5	37.6	56.7	59.2	77.0	81.4	18.8	35.5	60.0	60.0	83.9	58.5 (2)
LSTM-S2S-P	52.4	48.5	46.5	60.1	29.0	20.1	40.3	14.4	71.5	67.5	17.1	23.2	56.1	58.3	61.7	44.5 (18)
DeepAnt	50.6	62.0	37.7	65.9	40.8	28.4	52.0	47.0	75.5	68.1	19.2	29.1	61.3	60.2	63.8	50.8 (12)
TCN-S2S-P	47.2	73.3	44.6	65.5	57.7	42.6	51.6	42.3	78.8	84.5	27.2	37.2	61.6	60.0	85.5	57.3 (3)
GDN	57.8	58.3	40.9	64.9	58.6	29.2	52.7	41.5	67.9	72.5	18.0	33.8	61.6	55.4	74.5	52.5 (10)
LSTM-VAE	47.6	63.7	35.2	58.4	64.6	48.8	53.9	42.3	73.8	58.8	20.5	46.3	60.6	52.7	68.8	53.1 (9)
Donut	46.5	66.7	38.9	67.1	62.7	47.0	50.2	51.6	65.2	77.5	29.6	34.8	68.7	48.4	76.2	55.4 (6)
LSTM-DVAE	42.2	63.8	35.4	56.9	58.4	49.6	50.8	54.8	70.5	48.8	20.1	41.2	60.1	55.2	52.5	50.7 (13)
GMM-GRU-VAE	49.1	67.0	38.1	67.1	62.0	60.6	51.2	49.4	68.7	79.2	21.4	35.0	63.3	58.2	83.4	56.9 (4)
OmniAnomaly	45.3	67.7	35.3	65.3	42.9	57.7	62.0	40.7	77.0	57.1	16.9	25.7	56.8	44.6	82.4	51.8 (11)
SIS-VAE	52.6	65.7	38.4	65.4	50.8	30.9	52.9	49.0	74.9	73.0	21.2	32.8	58.1	63.8	79.1	53.9 (8)
BeatGAN	45.3	46.5	34.0	64.1	47.1	25.7	52.7	31.6	61.6	68.7	17.6	24.7	49.0	57.8	65.5	46.1 (16)
MAD-GAN	43.4	35.9	37.6	64.1	40.3	19.1	46.8	32.6	65.7	48.6	18.5	9.4	34.3	57.3	32.9	39.1 (23)
LSTM-VAE-GAN	47.9	46.9	31.0	67.9	44.4	23.1	56.3	17.8	57.1	56.6	16.1	19.5	37.9	61.6	69.8	43.6 (19)
TadGAN	49.0	27.3	22.9	64.1	45.4	22.0	54.4	23.9	64.0	63.3	16.6	18.7	54.5	62.2	49.5	42.5 (22)
LSTM-AE OC-SVM	19.0	28.2	24.6	49.3	13.3	23.4	23.5	8.4	50.7	61.6	14.6	8.8	40.5	60.4	67.3	32.9 (25)
MTAD-GAT	43.0	65.9	24.1	64.5	52.8	57.1	50.1	43.2	71.0	41.7	16.3	39.6	55.7	57.9	56.6	49.3 (14)

Table 12: Cross-validation results on SMD evaluated with our adapted AUPRC metric, using $TRec^*$ and $TPrec^*$.

	Server ID															
	1	6	8	9	10	11	13	14	16	17	20	21	24	26	27	avg.
LSTM-AE	39.5	70.9	25.6	29.2	65.5	33.8	46.1	59.2	48.8	81.1	17.8	37.1	64.9	31.0	81.8	48.8 (1)
LSTM-Max-AE	43.0	18.5	18.5	28.7	24.7	19.4	45.9	14.5	34.7	64.5	6.4	6.1	53.0	30.9	67.8	31.8 (20)
MSCRED	45.4	34.9	36.1	13.5	20.1	10.3	40.4	22.5	37.7	68.7	5.5	10.1	49.9	21.0	61.1	31.8 (19)
FC-AE	46.3	54.1	24.3	30.0	43.2	23.5	43.8	37.6	43.5	73.0	7.9	24.5	57.3	30.6	82.4	41.4 (8)
USAD	35.8	41.9	16.3	26.6	28.9	29.9	43.2	33.4	25.5	63.5	9.2	15.6	46.2	23.3	61.3	33.4 (16)
TCN-AE	25.8	30.5	19.0	8.5	12.0	12.5	20.0	9.2	37.1	56.3	9.4	10.3	34.0	31.5	36.1	23.5 (24)
GenAD	41.8	28.3	27.6	21.5	39.5	21.3	48.7	40.1	33.7	65.6	10.1	12.8	52.5	28.0	63.1	35.6 (14)
STGAT-MAD	42.6	61.1	23.7	30.1	56.6	27.2	45.3	48.6	47.6	77.2	15.7	24.9	62.9	33.5	80.4	45.2 (4)
LSTM-P	57.8	71.4	30.2	29.0	55.6	34.3	48.6	49.9	46.8	78.8	12.1	27.6	63.0	27.9	82.0	47.7 (2)
LSTM-S2S-P	45.5	37.3	33.5	13.9	22.4	12.4	36.6	10.1	38.5	59.6	8.1	15.3	50.1	27.7	56.9	31.2 (21)
DeepAnt	45.4	58.3	21.9	30.4	34.1	22.7	45.0	36.5	43.1	64.4	10.8	15.8	62.0	29.5	63.3	38.9 (10)
TCN-S2S-P	37.6	71.6	28.0	29.5	51.5	35.8	45.5	33.6	48.1	84.8	19.1	24.6	63.9	26.9	82.9	45.6 (3)
GDN	52.8	53.7	27.1	29.1	52.2	25.0	45.2	30.8	37.3	70.7	8.6	21.8	63.8	25.1	73.3	41.1 (9)
LSTM-VAE	32.5	53.8	18.3	25.5	56.1	44.0	47.0	27.5	40.2	53.6	12.7	29.2	57.6	18.5	62.6	38.6 (11)
Donut	33.0	59.9	20.0	29.8	58.3	40.0	40.6	41.3	36.0	75.0	19.7	25.0	69.4	15.0	73.8	42.5 (6)
LSTM-DVAE	26.8	55.6	16.9	20.5	46.3	46.4	43.7	37.4	38.0	40.7	12.0	24.3	56.9	21.7	46.4	35.6 (15)
GMM-GRU-VAE	37.4	60.6	20.8	31.6	51.1	56.3	43.9	39.8	36.0	75.7	12.5	18.0	64.6	27.4	81.1	43.8 (5)
OmniAnomaly	28.9	57.6	18.5	33.1	25.0	49.1	52.4	23.2	47.8	49.1	11.4	12.7	57.7	11.3	82.2	37.3 (12)
SIS-VAE	47.0	63.9	22.4	30.0	42.8	23.1	45.8	36.2	43.3	68.9	11.0	20.2	57.3	32.4	78.2	41.5 (7)
BeatGAN	39.8	39.8	21.3	26.1	38.6	20.1	43.6	20.2	29.4	64.2	8.4	15.7	42.7	27.4	57.6	33.0 (17)
MAD-GAN	33.3	26.6	18.7	27.1	33.4	14.8	24.8	19.7	33.8	48.3	7.7	4.4	25.6	25.5	31.4	25.0 (23)
LSTM-VAE-GAN	40.7	44.2	18.3	34.7	35.3	14.3	49.5	12.2	29.1	53.1	9.1	11.3	29.7	33.2	65.0	32.0 (18)
TadGAN	34.9	17.6	8.3	28.2	36.9	17.8	44.0	17.8	31.1	56.8	9.9	9.4	51.6	30.3	48.6	29.6 (22)
LSTM-AE OC-SVM	10.2	22.8	9.5	7.3	8.8	16.9	14.0	6.7	17.8	53.0	8.0	3.9	31.9	28.7	56.9	19.8 (25)
MTAD-GAT	31.1	65.6	10.4	27.3	46.8	54.1	42.5	32.2	37.0	34.8	10.6	30.1	53.9	23.0	53.3	36.8 (13)